

**FINITE ELEMENT ANALYSIS OF BIRD STRIKES ON COMPOSITE AND  
GLASS PANELS**

**KOH CHEE CHUAN**

**DEPARTMENT OF MECHANICAL ENGINEERING  
NATIONAL UNIVERSITY OF SINGAPORE**

**2005/2006**

FINITE ELEMENT ANALYSIS OF BIRD STRIKES ON COMPOSITE AND  
GLASS PANELS

SUBMITTED  
BY  
KOH CHEE CHUAN

DEPARTMENT OF MECHANICAL ENGINEERING

IN PARTIAL FULFILLMENT OF THE REQUIREMENTS FOR THE DEGREE OF  
THE BACHELOR OF ENGINEERING  
NATIONAL UNIVERSITY OF SINGAPORE

2005/2006

## **ABSTRACT**

In this final year project, a 1.82kg homogenous bird model with a simplified geometrical shape is modeled using the Lagrangian formulation. The reliability of the bird model is validated by comparing the numerical result with experimental results of a real bird of similar mass impacting normally at an impact velocity of 116m/s onto a flat rigid panel. Results are compared in terms of pressure profile, Hugoniot and stagnation pressure at the centre of the impact and the bird trajectory after the impact. The obtained numerical results are found to be comparable in terms of pressure profile and the bird trajectory. Numerical Hugoniot and stagnation pressure are higher by 33% and 20% respectively. This is attributed to the assumptions made in the formulation of the numerical model.

The modeling of bird strike using the Lagrangian Arbitrary Eulerian and Smooth Particle Hydrodynamics formulation is then investigated by modeling impact on an elastic aluminum panel. The verified Lagrangian model serves as a medium for comparison of the numerical results. The numerical results obtained from the various formulation shows close conformity implying their appropriateness as alternative in the simulation of bird strike.

The effect of curvature, of an aircraft windscreen, on the impact response in terms of effective stress at the center of the impact is also investigated. Analysis is made based on the obtained numerical results. However experimental results are not available to substantiate the conclusions made from the numerical results.

## **ACKNOWLEDGEMENT**

The author would like to thank his supervisor, Professor Lee Heow Pueh, for his guidance and advice rendered to him throughout the course of the final year project. The author is also grateful for the patience and understandings Professor Lee had given to him.

The author will also like to express his gratitude to Mr Tham Ching Yang for his help in the use of LS-DYNA and Truegrid<sup>R</sup>, the two software required to execute the project. The author is thankful for his patience and effort in answering the author's numerous queries.

The author would also like to extend his appreciation to all those who have helped him during the course of the project in one way or another.

<b>TABLE OF CONTENTS</b>	<b>PAGES</b>
<b>ABSTRACT</b>	<b>i</b>
<b>ACKNOWLEDGEMENT</b>	<b>ii</b>
<b>LIST OF FIGURES</b>	<b>v</b>
<b>LIST OF TABLES</b>	<b>viii</b>
<b>LIST OF SYMBOLS</b>	<b>ix</b>
<b>CHAPTER ONE – INTRODUCTION</b>	<b>1</b>
1.1 Background	1
1.2 Objectives	2
1.3 Scope	2
<b>CHAPTER TWO – LITERATURE REVIEW</b>	<b>4</b>
2.1 Background	4
2.2 Hazard Prevention	5
2.3 Bird Impact Testing	8
<b>CHAPTER THREE – MODELING METHODOLOGY</b>	<b>12</b>
3.1 General Parameters	12
3.2 Bird Model Verification	15
3.3 Evaluation of the Various Finite Element Formulations	18

3.4	Lagrangian Bird Model	19
3.5	Arbitrary Lagrangian Eulerian Bird Model	21
3.6	Smooth Particles Hydrodynamics Bird Model	24
3.7	Investigation of the Effect of Curvature on Impact Response Due to Bird Strike	26
<b>CHAPTER FOUR – RESULTS AND DISCUSSIONS</b>		<b>30</b>
4.1	Expected Results from Lagrangian Bird Model	30
4.2	Numerical Results from the Lagrangian Bird Model	32
4.3	Evaluation of the Various Finite Element Formulations	42
4.4	Effect of Curvature on Impact Response	50
<b>CHAPTER FIVE – CONCLUSIONS AND RECOMMENDATIONS</b>		<b>54</b>
5.1	Conclusions and Recommendations	54
<b>REFERENCES</b>		
<b>APPENDIX A</b>		
<b>APPENDIX B</b>		
<b>APPENDIX C</b>		
<b>APPENDIX D</b>		
<b>APPENDIX E</b>		
<b>APPENDIX F</b>		
<b>APPENDIX G</b>		
<b>APPENDIX H</b>		

---

<b>LIST OF FIGURES</b>	<b>PAGES</b>
Figure 2.1: Glaucous Gull, Gull Species, 2.4 – 4lb	6
Figure 2.2: (Left) Mallard, Waterfowl Species, 1.2 – 3.8lb, (Right) Gyrfalcon, Raptor Species, 2.2 – 4.4lb	7
Figure 2.3: Typical Pressure-Time Plot due to Impact on a Rigid Target from [12]	8
Figure 2.4: Pressure to Relative Volume Plot for Bird Material with Different Void Volumetric Fractions [11]	11
Figure 3.1: Geometry of Simplified Bird Model	12
Figure 3.2: Geometry of Rigid Plate	17
Figure 3.3: Lagrangian Bird Model and Rigid Plate after Reflection from the Quarter Model	19
Figure 3.4: Quarter Model and Corresponding Boundary conditions (Front View)	20
Figure 3.5: ALE Bird Model and Target	22
Figure 3.6: SPH Bird Model and Target	24
Figure 3.7: Cockpit Window for a Transport Aircraft [22]	27
Figure 3.8: Side View of Plate and Introduced Curvature	29
Figure 4.1: Pressure-Time Plot for Bird Impact on Rigid Plate at 116m/s [12]	31
Figure 4.2: Bird Trajectory of a SPH Bird Model after Impact [10]	31
Figure 4.3: Bird Trajectory of a Lagrangian Bird Model after Impact [12]	31
Figure 4.4: Pressure-Time Plot Obtained from the Lagrangian Bird Model	32
Figure 4.5: Bird Trajectory of Lagrangian Bird Model (In Direction Normal to the Plate)	33
Figure 4.6: Energy Plot (Lagrangian Bird Model)	34

---

Figure 4.7: Pressure-Time Plot (Left) and Energy Plot (Right) (Lagrangian Bird Model with Higher Mesh Density)	35
Figure 4.8: Pressure-Time Plot (Lagrangian Bird Model with Lower Time Step Scale Factor)	36
Figure 4.9: Pressure-Time Plot (Lagrangian Bird Model with Different Material Model) (Material of Porosity 0.1(Left), Material of Porosity 0.15 (Right))	38
Figure 4.10: Pressure-Time Plot (Lagrangian Bird Model with Different Material Model as Shown in Table 4.3)	38
Figure 4.11: Effective Stress Plot (A for Lagrangian, B for ALE, C for SPH)	43
Figure 4.12: Resultant Displacement Plot (A for Lagrangian, B for ALE, C for SPH)	43
Figure 4.13: Pressure Plot (A for Lagrangian, B for ALE, C for SPH)	43
Figure 4.14: Internal Energy Plot (A for Lagrangian, B for ALE, C for SPH)	46
Figure 4.15: Kinetic Energy Plot (A for Lagrangian, B for ALE, C for SPH)	46
Figure 4.16: Total Energy Plot (A for Lagrangian, B for ALE, C for SPH)	47
Figure 4.17: Bird Trajectory of SPH Bird Model (In Direction Normal to the Plate)	47
Figure 4.18: Bird Trajectory of ALE Bird Model (In Direction Normal to the Plate)	48
Figure 4.19: Impact Response of Transparency with no Curvature (A for Outer layer, B for Middle Layer, C for Inner Layer)	50
Figure 4.20: Impact Response of Outer Layer of Transparency (A for Flat Target, B for Target with 0.5m Radius of Curvature)	52
Figure 4.21: Impact Response of Middle Layer of Transparency (A for Flat Target, B for Target with 0.5m Radius of Curvature)	52
Figure 4.22: Impact Response of Inner Layer of Transparency (A for Flat Target, B for Target with 0.5m Radius of Curvature)	53
Figure G1: Effective Stress Plot (Lagrangian Model) (A for Coarser Mesh B for Denser Mesh)	G3

---

Figure G2: Resultant Displacement Plot (Lagrangian Model) (A for Coarser Mesh, B for Denser Mesh)	G3
Figure G3: Pressure Plot (Lagrangian Model) (A for Coarser Mesh, B for Denser Mesh)	G3
Figure G4: Effective Stress Plot (ALE Model) (A for Coarser Mesh B for Denser Mesh)	G4
Figure G5: Resultant Displacement Plot (ALE Model) (A for Coarser Mesh, B for Denser Mesh)	G4
Figure G6: Pressure Plot (ALE Model) (A for Coarser Mesh, B for Denser Mesh)	G4
Figure G7: Effective Stress Plot (SPH Model) (A for Lesser Particles B for More Particles)	G5
Figure G8: Resultant Displacement Plot (SPH Model) (A for Lesser Particles, B for More Particles)	G5
Figure G9: Pressure Plot (SPH Model) (A for Lesser Particles, B for More Particles)	G5
Figure H1: Effect of Curvature on Effective Stress (Outer Layer) (A for plate2, B for plate3, C for Plate4, D for Plate 1, E for Plate 5)	H2
Figure H2: Effect of Curvature on Effective Stress (Middle Layer) (A for plate2, B for plate3, C for Plate4, D for Plate 1, E for Plate 5)	H2
Figure H3: Effect of Curvature on Effective Stress (Inner Layer) (A for plate2, B for plate3, C for Plate4, D for Plate 1, E for Plate 5)	H2

<b>LIST OF TABLES</b>	<b>PAGES</b>
Table 3.1: Summary of Parameters Affecting Bird Strike and Respectively Values Chosen	13
Table 3.2: Summary of Parameters Used and Respectively Values Chosen	16
Table 3.3: Properties of Aluminum Plate	18
Table 3.4: Penalty Stiffness Defined for the Contact Card	21
Table 3.5: Properties of Acrylic Layer [23]	28
Table 3.6: Properties of PVB Layer [21]	28
Table 3.7: Plate Number and Introduced Curvature	29
Table 4.1: Expected Hugoniot and Stagnation Pressure [12]	32
Table 4.2: Parameters of Other Bird Material Used	37
Table 4.3: Final Results Obtained from the Lagrangian Bird Model	40
Table 4.4: Mesh Density and Computational Time for the Various Bird Model	49
Table A1: Weight of Some North American Gull Species [4]	A1
Table A2: Weight of Some North American Water Fowl Species [4]	A1
Table A3: Weight of Some North American Raptor Species [4]	A2
Table G1: Mesh Density and Computational Time for the Various Bird Model	G1

**LIST OF SYMBOLS**

P	Pressure
$P_H$	Hugoniot Pressure
$P_S$	Stagnation Pressure
$\mu$	Miu
$\rho$	Density
$\rho_o$	Initial Density of Material
E	Internal Energy Per Volume
$\alpha$	Void Volumetric Fraction (Porosity) for Bird Material
$v_r$	Relative Specific Volume
$v_o$	Initial Specific Volume of Material
v	Current Specific Volume of Material
u	Translation in x Direction
v	Translation in y Direction
w	Translation in z Direction
$\theta_x$	Rotation about x Axis
$\theta_y$	Rotation about y Axis
$\theta_z$	Rotation about z Axis
DOFs	Degree of Freedoms
K	Bulk Modulus
P.S	Penalty Stiffness

E	Young's Modulus
W	Kernel Function
m	Mass
x	Position of SPH Particle

## ***CHAPTER ONE - INTRODUCTION***

### **1.1 BACKGROUND**

Bird strikes have been a concern to both civil and military aircrafts. Since 1988, such incidents have claimed the life of over 195 people [1]. In United States alone, more than 50,000 incidents of bird strikes were reported between 1990 and 2003.

The front facing components of an aircraft which include the nacelles, windshield, wind leading edge, compressor blade, etc are often most susceptible to such strikes. It is therefore critical to ensure that the different structural parts are able to withstand such high velocity impact or at least guarantee the safe landing of the aircraft after the strike.

Certification standards, which include verifying the structural integrity of airframes and engines, are established by U.S. Federal Aviation administration (FAA) and European Joint Aviation Authority (JAA) [2]. These empirical verifications, which result in the damage of prototypes and the biological hazard of using real birds, can be costly and time consuming. The use of computer simulation to simulate the bird impact on new structural components serves as a powerful tool for the development of new components by minimizing the number of empirical testings. It allows the impact response of different structural and material parameters to be studied before the actual fabrication of the prototypes, thus reducing time and cost incurred in empirical testing.

## **1.2 OBJECTIVES**

The objective of the final year project includes

- 1) Obtaining a realistic finite element bird model with the help of scattered reported studies.
- 2) Investigating the modeling of bird strike using 3 different formulations namely, Lagrangian, Arbitrary Lagrangian Eulerian (ALE) and Smooth Particle Hydrodynamics (SPH) formulation.
- 3) Investigate what effect curvature, of an aircraft windscreen, has on the impact response due to bird strike.

## **1.3 SCOPE**

In this final year project, the finite element simulation was performed using LS-DYNA.

A 1.82 kg, homogenous bird model with a simplified geometrical shape was modeled.

The reliability of the bird parameters was validated by simulating collision of the Lagrangian bird model at 90° onto a flat rigid panel at an impact velocity of 116m/s and comparing with reported experimental data. Parameters used for the assessment of the validity of the bird model include the pressure profile at the centre of the impact as well as the bird trajectory after the impact.

Evaluation of the 3 different finite element formulations, namely Lagrangian, ALE and SPH in the analysis of bird strike was made by simulating impact of the bird models on an elastic aluminum flat panel. The numerical results chosen for comparison include the plot of effective stress, resultant displacement and pressure at the centre of the aluminum plate. Other aspects that are compared include the bird trajectory after the impact, the ease of modeling and the computational time required.

Finally the effect of curvature, of an aircraft transparency, on the impact response was investigated. The study focuses on relative comparison of the effect of curvature instead of the actual impact response due to bird strike.

.

## ***CHAPTER TWO – LITERATURE REVIEW***

### **2.1 BACKGROUND**

The studies of bird strikes can generally be classified into 2 categories namely hazard prevention and bird impact testing.

Hazard prevention involves collecting data from cases of bird strikes on aircraft and implementing measures to prevent them through the better understanding of the nature of strikes. This includes knowing the type of birds, the location, time of the day, season of the year, etc whereby the strike occurs.

Although measures have been implemented to prevent bird strikes from occurring, it is impossible to prevent them totally. It is therefore important to ensure that impact response on the aircraft are fully understood so as to give assurance to the pilot, passenger, etc in cases where strikes occur. This is done through bird impact testing.

Bird impact testing consists of empirical studies as well as numerical studies. Through bird impact testing, new engines and airframes are subjected to simulated and actual bird strikes. Certification of new aircraft parts are usually done empirically. These testing can be expensive and time consuming hence preliminary studies are usually done by numerical simulation before actual empirical testings.

## **2.2 HAZARD PREVENTION**

Collision between aircraft and bird has been a concern because they threaten the safety of the people on board the aircraft, results in costly repairs and in the case of commercial aircraft, a loss in revenue. It is a hazard that threatens to weaken the public confidences towards the aviation industries. International committees such as the International bird strike committee, the U.S and Italian bird strike committee, etc [3], have been formed to counter the threat posed by bird strikes, to better understand the nature of strikes and to implement measures to prevent such strikes.

Since 1988, over 195 people have been killed world-wide as a result of bird strikes [3]. Bird strikes are not rare cases as most people professed. In the United States alone, 52,493 strikes have been reported from 1990 to 2003. Within this 14 years period, 244,510 hours of aircraft down time and \$163.51 million were loss. Analysis of strike reports has shown that the number of reported strikes constitutes only about 20% of the total number that truly occur which means that the amount of monetary losses can be much more than what is actually estimated [3 - 4]. Bird strike is therefore a much more serious problem than what most people perceived especially when the numbers of aircraft are increasing every year and becoming faster and quieter.

Generally, the number of reported strike decrease with altitude. Jetliners normally cruise at about 35,000 feet (10000m) at speeds over 500 miles per hour (224 m/s). They usually take off and land at a speed of up to 235 miles per hour (105 m/s) [6]. Reported studies [4

- 5] show that it is near the airport where aircraft are most vulnerable to bird strikes. Birds are attracted to airport due to the presence of shelter, feeding, drinking and bathing areas. In United States, 92% of the strikes occur at below 3000 feet (920m) and a total of 97% of the reported strikes occur during the taking off and landing phase of the aircraft [4]. Due to the higher proportion of strikes at take off and landing, the impact response on aircraft components, windshield, engine compressor, etc, at an impact speed of around 105m/s is therefore much studied experimentally and numerically.

The species of bird that commonly strike the aircraft varies from country to country. Of the strikes that had been reported in United States, the Waterfowl (32%), gulls (28%),

and raptors (17%) represented 77% of the reported bird strikes causing damage to USA civil aircraft, 1990-2 [3]. Bird sizes cover a considerable range which differs for different groups as well as different species Refer to appendix A for the general weight of the different species pertaining to the



Figure 2.1: Glaucous Gull, Gull Species, 2.4 – 4lb

different groups of birds. Generally,

the heavier the bird the greater will be the risk for serious aircraft damage. Figure 2.1 and 2.2 shows some of the common group of birds that are involve in the collision with aircrafts.

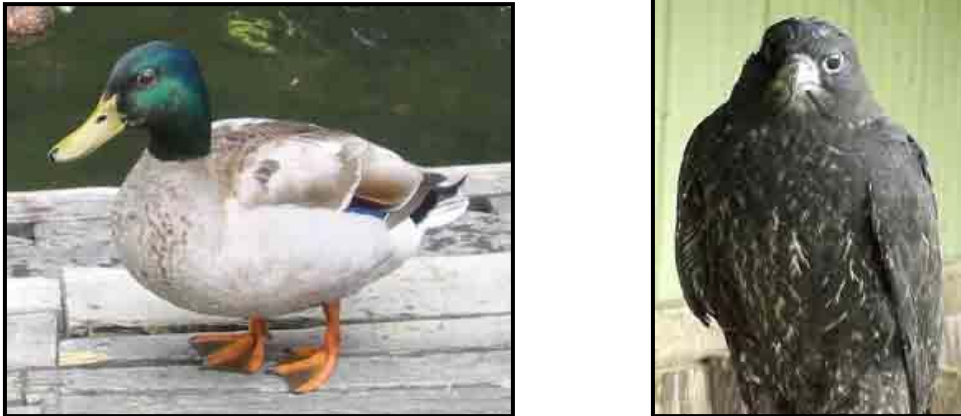


Figure 2.2: (Left) Mallard, Waterfowl Species, 1.2 – 3.8lb (Right) Gyr falcon, Raptor Species, 2.1 – 4.4lb

Airframes and engines airworthiness standard are certified by the Federal Aviation Administration (FAA) and the European Joint Aviation Authority (JAA). Due to the large variety of birds, which vary in size and weight, that are involved in bird strikes, it is not possible to ensure the airworthiness of an airframe or engine for any particular type of bird. An optimum standard is therefore chosen after weighing the various factors which includes the probability and severity of strikes, the aircraft operating environment, as well as the economic cost involved in implementing the standard. One of the requirements for airframes by the FAA for transport category aircraft requires that the aircraft be able to successfully complete a flight after impact with a 4lb (1.82kg) bird [2]. The use of bird weighing 1.82kg is therefore used for impact testing in a number of experimental and numerical studies.

### 2.3 BIRD IMPACT TESTING

Similar to bird strike certification process, experimental studies of bird strike are usually conducted by firing euthanized birds, usually chicken carcass, from gas cannon onto a target structure at designated speed. However unlike in certification test, experimental studies tested with alternative material such as gelatin, as substitute for real bird. The similarity in spatial and temporally pressure distribution on a rigid target from impact by a real bird and artificial bird of gelatin material suggest that gelatin behaves in a similar manner to real bird during impact [13 - 15]. High speed firms are used to monitor the deformation of the target and the bird trajectory at different phase of the impact. Pressure distribution and deformation on the target due to the impact are measured by mounting of suitable pressure transducer and strain gauges on the target.

Generally pressure-time plot from a rigid target due to bird impact are distinguished by a few characteristics as reported by [9]. It was found that the pressure-time plot due to impact is characterized by a higher frequency pressure superimposing onto a lower frequency pressure as shown in figure 2.3 for example.

The pressure time plot starts with a quick rise to an initial peak pressure known as the Hugoniot pressure followed by pressure decay and then a substantial period of

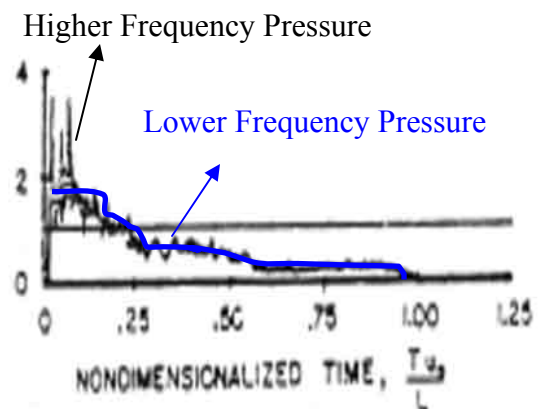


Figure 2.3: Typical Pressure-Time Plot due to Impact on a Rigid Target [12]

steady state pressure known as the stagnation pressure. The amplitude of the pressure falls with increasing radial distance from the centre of impact. Various reported numerical studies of bird strike have documented the use of bird impact on rigid targets to validate the parameters of their finite element bird model. They obtain pressure time plot of comparable characteristics as discussed earlier [10 – 12].

Numerical simulation of bird strikes can be accomplished by a number of commercially available finite element software which include, PAM-SHOCK [7], LS-DYNA [8], etc. Before the Arbitrary Lagrange Eulerian (ALE), and the Smooth Particle Hydrodynamics (SPH) algorithm are available in commercial finite element software, Lagrangian bird model had been an established method in the computational simulation of bird strike. However stability problem associated with the Lagrangian bird model had been reported in a number of studies [11 - 12]. Large element distortions in the model of the bird ultimately leads to numerical errors. To tackle the problem, Airoldi and Cacchione [11] adopted a numerical strategy which removed the hydrodynamic material response in zones where numerical errors occurred. In recent years, alternative numerical methods such as the ALE, and the SPH method had been explored to address the stability problem posed by the Lagrangian method and to better model the bird trajectory after impact. So far, no stability problem had been reported for numerical studies using ALE and SPH formulation.

Lagrand *et al.* [12] modelled bird impact onto rigid targets using both the Lagrangian and ALE formulation in Radioss [17]. Results of the ALE model were found to be close to

Lagrangian ones in terms of local pressure and global load. The simulation time is also found to be lower for the ALE formulation compared to the Lagrangian model. Hannsen [16] used the ALE formulation to simulate bird strike on foam-based sandwich panels. The bird was modelled using ALE formulation while the sandwich panel modelled using a Lagrangian approach. Simulated results were compared with experimental ones in terms of strain and deformation behaviour of the sandwich panel. The results were found to compare well for the first milli-seconds of the event.

Other authors [10][13 - 14] used SPH method to model the bird, in which the finite element mesh is replaced by interacting particles. Alastair *et al.* [10] managed to show for an impact on a rigid target, a good agreement in the pressure pulse data between experimental and numerical result could be obtained. McCallum and Constantinou [13] on the other hand showed a good general agreement between ALE and SPH formulation for impact on an aluminum deformable plate. In [14], the SPH model was used in an impact on an aircraft wing leading edge structure. The SPH bird model was able to capture the breakup of the bird into debris particle after its collision with the wing leading edge structure, something that was difficult to accomplish using the Lagrangian method.

The shape of the bird is usually represented as a cylinder with two hemispherical ends as in most instances; such simple geometry represents the torso of the bird [10 - 14]. Other shapes that had been experimented before include cylindrical [11] and spherical shape. Other than the simplified models, [13] modeled a multi-material bird taking the influence of head and neck during impact for larger birds into consideration.

Due to the rapid deceleration at the point of impact, the material response of the bird models can be treated as a fluid as the yield stress of the bird material is greatly exceeded on impact. The bird material had been characterized as a viscous hydrodynamic fluid in [12][16]. Considering that the structure of real birds usually consists of some internal cavities such as lungs, some authors had taken the effect of porosity into consideration in the modeling of bird strike [11][18]. Figure 2.4 presents the pressure to relative volume plot for bird material with void volumetric fractions,  $\alpha = 0.00, 0.10$  and  $0.15$ . Porosity affects the Hugoniot and stagnation pressure.

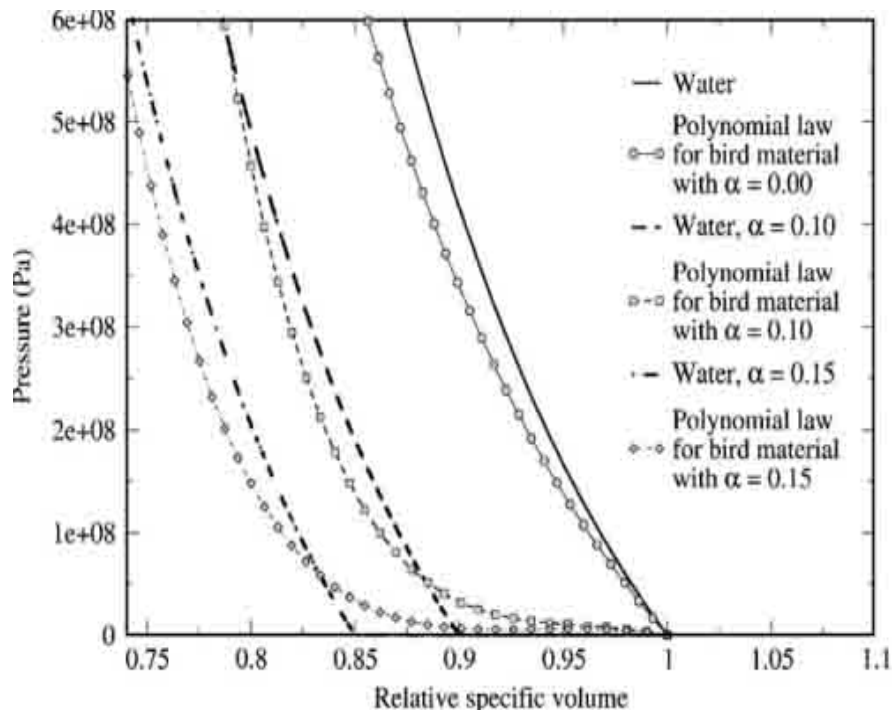


Figure 2.4: Pressure to Relative Volume Plot for Bird Material with Different Void Volumetric Fractions [11]

In this final year project, as experimental studies were not carried out, the parameters of the bird model and the results used to verify the bird model is obtained from earlier published reports.

## ***CHAPTER THREE – MODELING METHODOLOGY***

### **3.1 GENERAL PARAMETERS**

The finite element analysis of the bird strike is performed using LS-DYNA whereby its main solution methodology is based on explicit time integration. Explicit methods are more efficient compared to implicit method for fast phenomenon such as impact [19]. The keyword format is used for the input deck. The finite element mesh of the bird and the target is generated using TrueGrid<sup>R</sup> [20]. The parameters discussed in this section apply to all 3 numerical formulations investigated, namely Lagrangian, ALE and SPH. The extent of damage that results from bird impact is governed by several parameters. Some of the more important parameters together with the respective assumptions made or values chosen for this final year project are summarized in table 3.1. The reasons for choosing the various parameters are discussed subsequently. It should be noted however that the choice of the parameters is dependent on the availability of experimental results with similar bird parameters to compare against.

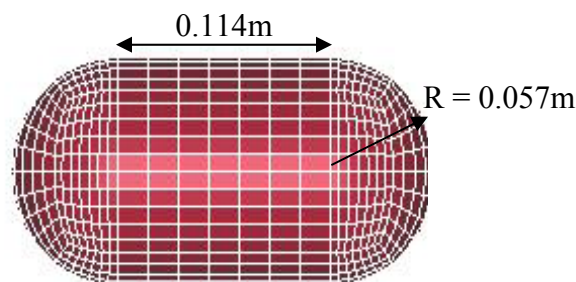


Figure 3.1: Geometry of Simplified Bird Model

Table 3.1: Summary of Parameters Affecting Bird Strike and Respective Values Chosen

No.	Parameters Governing the Impact Response of Bird Strike	Assumptions or Values Chosen
1	Bird Mass	1.82 kg
2	Bird Geometry	Cylinder with Hemispherical Ends (Figure 3.1)
3	Bird Density	938.5kg/m <sup>3</sup>
4	Bird Material	Viscous Hydrodynamic Fluid

As shown in table 3.1, the shape of the bird is chosen to be a cylinder with two hemispherical ends. This simplified geometry represents the torso of the bird and is commonly used in the numerical studies of bird strike. In conjunction with the certification standard required by the FAA for transport category aircraft, the mass of the bird model is chosen to be 1.82 kg. The density of the bird model on the other hand is chosen to be 938.5 kg/m<sup>3</sup> after taking into consideration that avian tissue are composed mainly of water with a small percentage of internal cavities such as lungs. With a mass of 1.82 kg and a density of 938.5 kg/m<sup>3</sup>, the dimensions of the bird is calculated and shown in figure 3.1. It has a length to diameter ratio of 2:1.

The pressure distribution on the target due to impact is dependent on the constitutive response of the bird model. A fluid like hydrodynamic response is chosen for the bird

material as it best represents the impact regime due to bird strike. As seen from figure 2.4, the constitutive response of the hydrodynamic bird model can be represented by a curve relating the pressure to the relative volume at different stage of the impact. This curve can be represented by a polynomial equation involving pressure and relative volume. The fluid like hydrodynamic response of the bird material model is defined by card \*MAT\_NULL and equation of state by card \*EOS\_LINEAR\_POLYNOMIAL in LS-DYNA. \*MAT\_NULL card can be used to represent fluid like material. In the \*MAT\_NULL card, the material identification of the bird model is defined. The density as well as the viscosity of the fluid representing the bird is also defined in this card. The null material model must be used with an equation of state that is defined by a separate card. The card \*EOS\_LINEAR\_POLYNOMIAL is chosen. In this card, the relationship between pressure and  $\mu$  is represented by a third order polynomial equation given by

$$P = C_0 + C_1\mu + C_2\mu^2 + C_3\mu^3 + (C_4 + C_5\mu + C_6\mu^2) E \text{ -----(1)}$$

$$\text{Where } \mu = (\rho / \rho_0) - 1 \text{ -----(2)}$$

Figure 2.4 shows various curves that governs the constitutive response of the bird material. It is a plot of pressure to relative specific volume  $v_r$ .

$$\text{Since } v_r = (v / v_0) = (\rho_0 / \rho) \text{ ----- (3)}$$

It can be shown with some arithmetic that equation 1 and hence \*EOS\_LINEAR\_POLYNOMIAL can be used to define the curve in figure 2.4 and hence the constitutive response of the bird model. In this final year project, the bird material is assumed to be a viscous hydrodynamic fluid as adopted by [12][16] whereby the coefficients of equation 1 is given by

$$C_n = 2250 \text{ MPa} \quad \text{for } n = 1 \text{ and } 0 \text{ otherwise} \quad \text{-----} \quad (4)$$

Results of the simulation are generated every 0.01ms. This to ensure that sufficient resolution is given to capture the initial peak of the Hugoniot pressure which occurs within a time frame of approximately 0.02 ms. A maximum scale factor of 0.9 is set for the time step to minimize computational time but yet ensure stability.

### **3.2 BIRD MODEL VERIFICATION**

The reliability of the various parameters discussed earlier is first validated by simulating bird impact at a velocity of 116m/s on a rigid, flat panel using a Lagrangian bird model. The experimental results in terms of Hugoniot, stagnation pressure and the pressure profile at the centre of the rigid targets are obtained from [12] for comparison (Refer to section 4.1 for more details). A rigid target instead of a deformable one is chosen for the validation so that the bird parameters can be determined independent of the constitutive response of the target. A normal impact and a flat panel are chosen so as to simplify the modeling procedure and to introduce less disparity between numerical and experimental

conditions. The parameters are summarized in table 3.2. To a certain extent, any major difference between the numerical and experimental result will then most likely be attributed to the inaccuracy of the assumed bird parameters.

Table 3.2: Summary of Parameters Used and Respectively Values Chosen

<b>No.</b>	<b>Parameters Used</b>	<b>Assumptions or Values Chosen</b>
<b>1</b>	Angle of Impact	Normal to Impacted Surface
<b>2</b>	Impact Velocity	116m/s
<b>3</b>	Shape of Impacted Surface	Flat Surface
<b>4</b>	Rigidity of Impacted Surface	Rigid / Deformable

The finite element mesh of the rigid target is created using 4900 evenly distributed shell elements. Shell element is used since the thickness of the plate is much smaller (70 times) compared to its other dimensions. Figure 3.2 shows the geometry of the rigid plate.

The dimensions and mesh density chosen is arbitrary. The boundary of the rigid target is set by constraining the node's rotational and translational degree of freedoms at the edge of the plate. The material property of the rigid plate is defined by card \*MAT\_RIGID. Card \*MAT\_RIGID provides a convenient way of turning one or more parts consisting of beam, solid or shell elements in LS-DYNA into a rigid body.

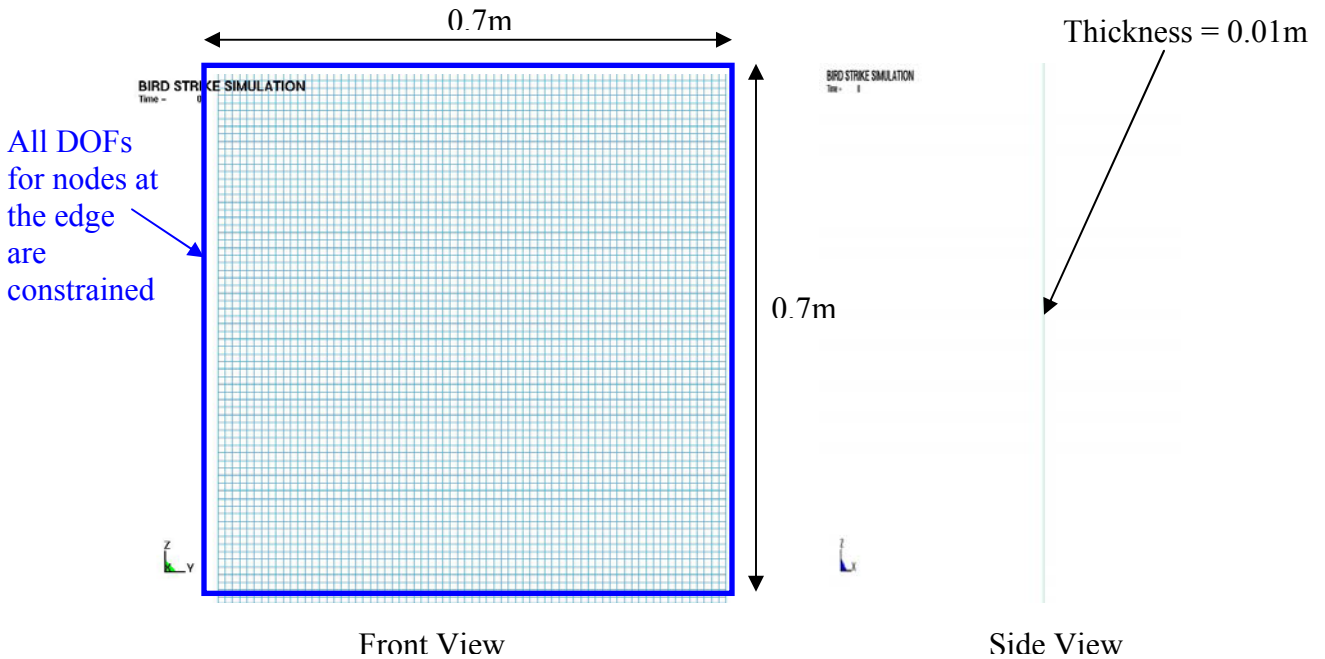


Figure 3.2: Geometry of Rigid Plate

Elements which are rigid are bypass in the computation and no storage is allocated for any variables related to the rigid body. On one hand, this material type is cost efficient as it reduces computational time and it allows one to model a rigid target without going through the hassle of having to model a thick plate or assuming a plate with high stiffness. On the other hand, since pressure is a function of displacement, the assumption of perfect rigidity means that the pressure profile could not be obtained from the plate itself. A way to go round this problem is to obtain the pressure profile from the tip of the Lagrangian bird model itself. This is reasonable since base on Newton's third law, an action produce equal and opposite reaction, the force exerted and hence pressure exerted by the bird on the plate and by the plate on the bird at the centre of the target should be the same. It should be noted however that the pressure profile is dependent to a certain extent on the mesh distribution of the Lagrangian bird model.

### **3.3 EVALUATION OF THE VARIOUS FINITE ELEMENT FORMULATIONS**

After validating the bird parameters as discussed in section 3.1; geometry, constitutive response, etc, that defines the bird model with the Lagrangian formulation, the bird parameters can be assumed to be valid and applied to the ALE and SPH bird model. Table 3.2 summarizes the values of the other parameters adopted. The Lagrangian bird model can serve as a medium for comparison with the ALE and SPH model. Since the 3 different bird models are created by different formulations, a more reasonable mean of relating the 3 models would be to obtain the pressure profile from the target instead of the bird so as to provide a common datum for comparison. For comparison sake, the target is remodeled to assume the property of a deformable aluminum plate. The geometry and mesh density remains unchanged. The card \*MAT\_ELASTIC defines the property of the deformable aluminum target. The \*MAT\_ELASTIC card defines isotropic elastic material and is defined for beam, solid and shell elements. Deformable aluminum plate is used as information with regards to the property of aluminum is readily available. The various values used to define property of aluminum are shown in table 3.3.

Table 3.3: Properties of Aluminum Plate

<b>No.</b>	<b>Properties of Aluminum Plate</b>	<b>Values Chosen</b>
<b>1</b>	Mass Density	2700 kg/m <sup>3</sup>
<b>2</b>	Young's Modulus E	70 e9 Pa
<b>3</b>	Poisson's Ratio	0.3

Sections 3.4 to 3.6 discuss the modeling of the bird specific to each of the formulations.

### 3.4 LAGRANGIAN BIRD MODEL

In the Lagrangian formulation, the material is bounded to the mesh, the mesh followed the distortion and movement of the material. Due to symmetry, the Lagrangian bird model can be represented using a quarter model. Figure 3.3 shows the initial position of the Lagrangian bird model and the rigid target. The bird model is position as close to the target as possible. For an impact velocity of 116m/s, the time taken for the whole bird to fully impact the rigid plate is 2.05ms. A termination time of 2.1ms is set in card \*CONTROL\_TERMINATION as any longer time would have wasted unnecessary computer resources. The quarter bird model is initially assigned with a mesh of 525 constant stress, hexahedral elements with finer mesh defined at the impacting end of the bird model so as to better capture the pressure distribution near the tip of the bird.

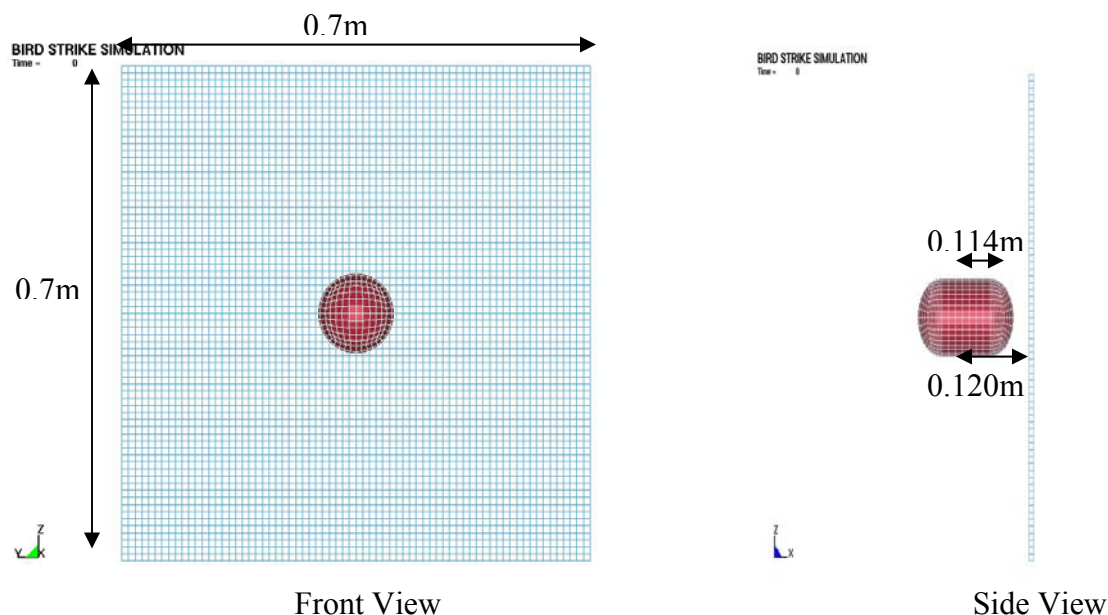


Figure 3.3: Lagrangian Bird Model and Rigid Plate after Reflection from the Quarter Model

The boundary condition of the quarter bird is defined as shown in figure 3.4.

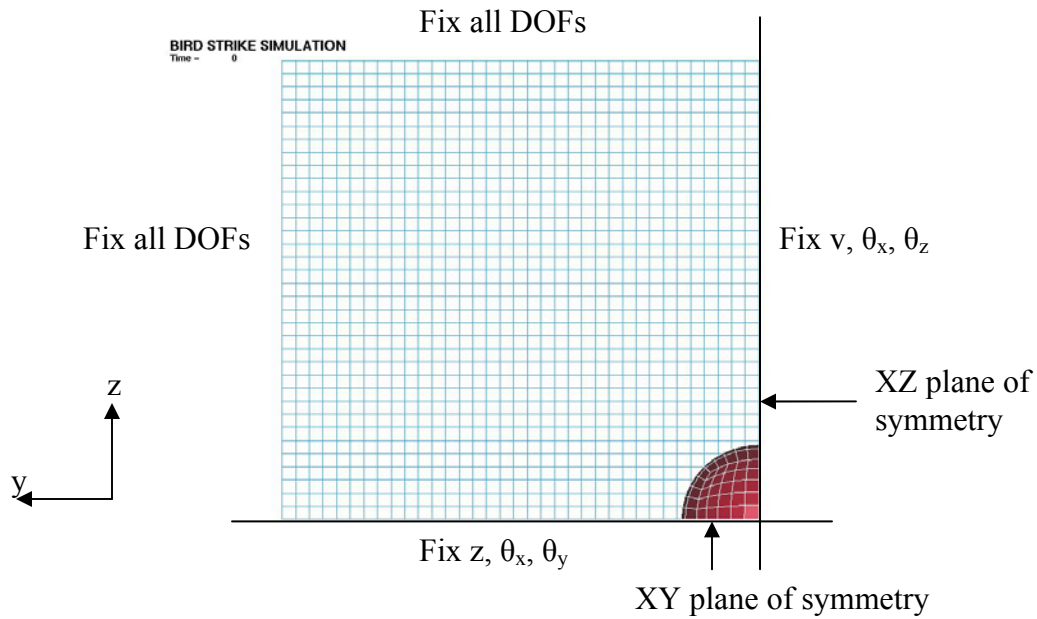


Figure 3.4: Quarter Model and Corresponding Boundary conditions (Front View)

The coupling between the Lagrangian bird and the target is represented using a surface to surface contact algorithm defined by the card \*CONTACT\_AUTOMATIC\_SURFACE\_TO\_SURFACE. Using this contact card, the coupling between the bird and target is base on a penalty method whereby the amount of penetration between the slave and master side is governed by penalty stiffness. The required penalty stiffness can be calculated using the relationship between the bulk modulus between the slave and master part shown in equation 5. Incorrect penalty stiffness can lead to excessive penetration of the bird model into the rigid plate which eventually results in numerical errors. For the contact card chosen, it does not matter which side is defined as the slave and which side is defined as the master.

$$K_{slave} \times P.S_{slave} = K_{master} \times P.S_{master} \text{-----} (5)$$

Taking the bird as the slave part and the target as the master part and using the default penalty stiffness of 0.1 for the master part, the required penalty stiffness for the slave part to avoid penetration is calculated and shown in table 3.4.

Table 3.4: Penalty Stiffness Defined for the Contact Card

<b>Part</b>	<b>Bulk Modulus K</b>	<b>Penalty Stiffness</b>
Bird (Slave)	2.2 e9 Pa	2.6515
Aluminum Rigid Target (Master)	58.33 e9 Pa	0.1

This section discusses the initial formulation of the Lagrangian bird model. After comparison with experimental results, refinements are made to the bird model. This will be further discussed in section 4.2. The LS-DYNA keyword file of the Lagrangian model is attached in appendix B.

### **3.5 ARBITRARY LAGRANGIAN EULERIAN BIRD MODEL**

In the ALE formulation, each element is allowed to contain more than one material. In this model, the bird is modeled to be surrounded by air pressurized at 1 bar. Unlike in Lagrangian formulation, the material does not always follow the distortion and movement of the mesh but instead is rezoned at each advection phase. Since the material does not follow the movement of the mesh, a boundary condition cannot be applied to the material representing the bird making the modeling of a quarter bird an unfeasible option. A full

bird is therefore modeled despite a present of symmetry. Figure 3.5 show the initial position of the ALE bird model and the target.

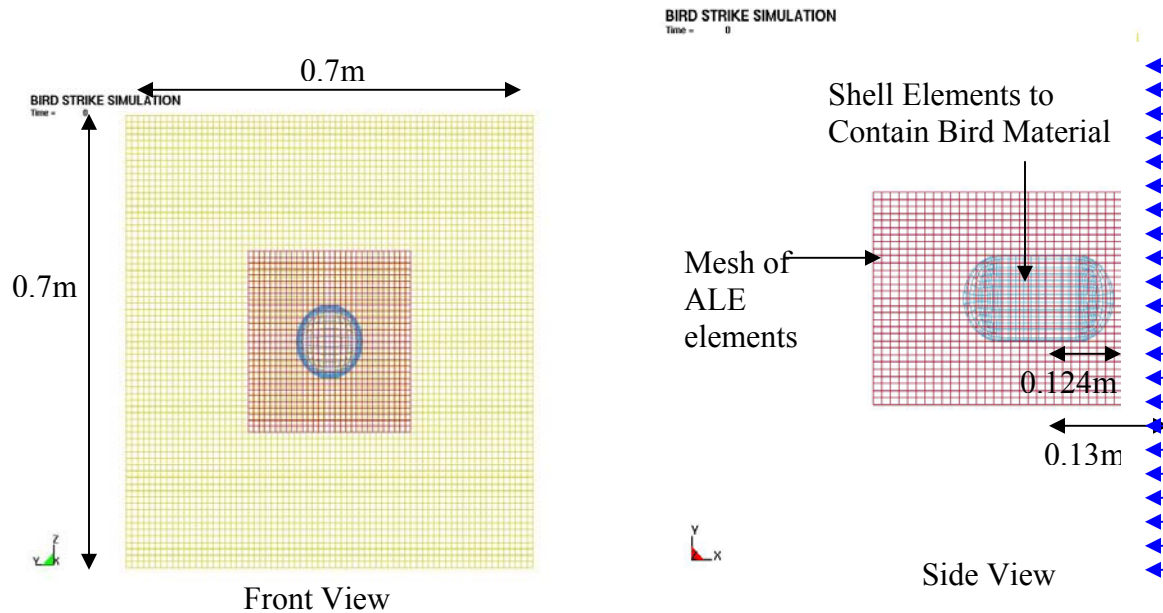


Figure 3.5: ALE Bird Model and Target

The bird material is position as close to the target as possible. Care is taken to ensure that the mesh is big enough to contain the bird material regardless of the distortion of the material throughout the simulation. For an impact velocity of 116m/s, the time taken for the whole bird to fully impact the rigid plate is 2.1ms. A termination time of 2.15ms is set in card \*CONTROL\_TERMINATION.

The bird initial geometry and position is defined by a mesh of shell elements. Card \*INITIAL\_VOLUME\_FRACTION\_GEOMETRY fills the inside of the shell with the fluid representing the bird model, the outside of the shell with air and the intersection with a partial volume. Care should be taken in defining the orientation of the normal

vectors belonging to the shell elements as an inconsistent definition with those defined in the card will result in the spillage of the material outside the intended volume. The volume fraction card is supposed to be defined together with card \*ALE\_MULTI\_MATERIAL\_GROUP. Card \*ALE\_MULTI\_MATERIAL\_GROUP defines the different groups of material within the ALE elements. The same group of material will coalesce when they flow into the same element. Two groups of material namely air surrounding the bird and the fluid representing the bird is defined. The multi-material card ensures that there is a boundary distinction between the two different groups of materials throughout the simulation. The bird and the surrounding air is modeled using an initial mesh of 3528 ALE elements. In order to contain the bird material within the mesh throughout the simulation and to avoid modeling an excessive large mesh which will increase the computational time, the mesh is allowed to translate and expand with the help of card \*ALE\_REFERENCE\_SYSTEM\_GROUP.

The coupling between the ALE formulated bird model and the Lagrangian formulated rigid plate is activated by card \*CONSTRAINT LANGRANGE IN SOLID. This card provides the mechanism for coupling interaction between a (slave) Lagrangian geometric entity to a (master) ALE entity. The normal vector of the Lagrangian formulated plate should be pointed in the direction of the fluid to be coupled as shown by the blue arrows in figure 3.5. The ALE elements and the Lagrangian shell elements will not interact otherwise. Another thing to note about the card \*CONSTRAINT LANGRANGE IN SOLID is the number of coupling points assigned to the surface of each Lagrangian element. NQUAD in the card defines the number of control points to detect penetration

between the contact entities. Leakage will occur if there are insufficient control points. NQUAD is generally 2 to 3 per ALE element. NQUAD is defined depending on the number of Lagrangian elements spanning each ALE element. The LS-DYNA keyword file of the ALE model is attached in appendix C.

### 3.6 SMOOTH PARTICLE HYDRODYNAMICS BIRD MODEL

SPH is a mesh free numerical method unlike the Lagrangian and ALE formulation. The material is represented by a set of discrete particles. Truegrid<sup>R</sup> cannot generate a gridless model. To model the SPH bird, a finite element mesh is first generated in Truegrid<sup>R</sup> and then manually converted to sets of discrete particles within the input deck. A full SPH bird is modeled. Figure 3.6 shows the initial position of the SPH bird model and the target captured from LS-PREPOST.

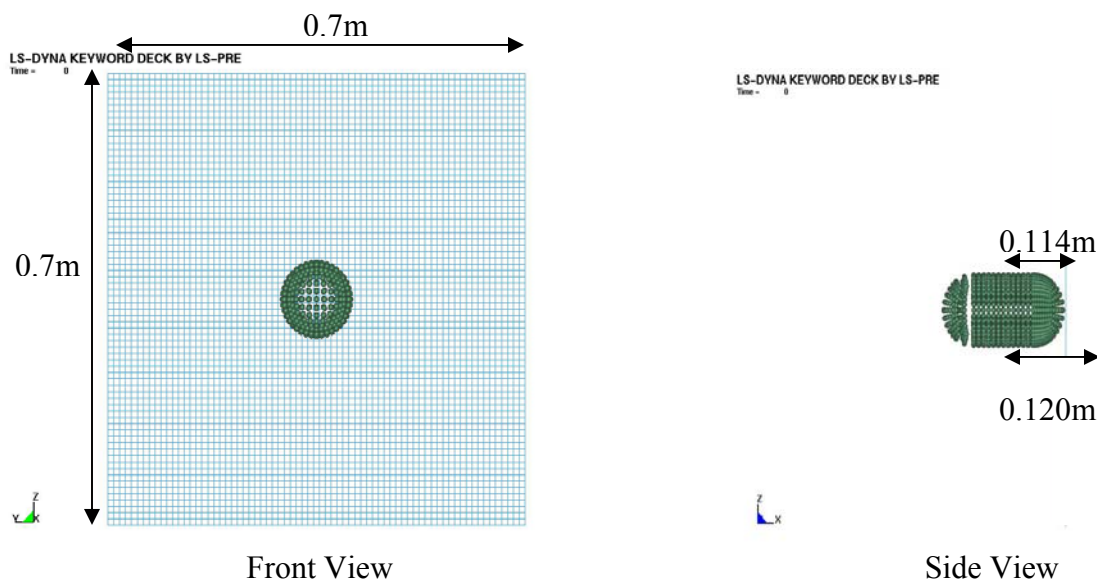


Figure 3.6: SPH Bird Model and Target

The initial position of the SPH bird model is similar to the Lagrangian bird model except that the elements are replaced by particles. A termination time of 2.1ms is set in card \*CONTROL\_TERMINATION.

For SPH formulation, the property of a particle of interest could be obtained by the property of its surrounding particles which is governed by the kernel function and the smoothing length. The property of any particle can be obtained by summing the relevant properties of other particles which lies within a radius of 2 smoothing length. The quantity A of any particle i represented by  $A_i$ , can be represented by the equation

$$A_i(r) = \sum m_j (A_j/\rho_j) W(x_i - x_j, h) \text{-----}(6)$$

Where  $x_i$  and  $x_j$  are the location of particles i and j respectively.  $m_j$  and  $\rho_j$  are the mass and density associated with particle j. W is the kernel function which is a function of the smoothing length and the position of the relevant particles. The contribution of each particle to the particle of interest is weighted by the kernel function.

The SPH processor in LS-DYNA uses a variable smoothing length, keeping the same number of particles in the neighborhood of the particle of interest. The maximum and minimum value which this smoothing length varies can be defined in card \*SECTION\_SPH. Using a variable smoothing length optimize the computation in the region of interest whereby the smoothing length is decrease for denser region and vice

versa. For the SPH bird model, the scale factor for the maximum and minimum smoothing length is set at 0.2 and 2 respectively.

A box is defined in the card \*CONTROL\_SPH. Particle approximation is computed for particles within the defined box. Particles that are outside the box are deactivated. This saves computational time as particles that no longer interact with the structure are eliminated.

The coupling between the SPH bird model and the target is represented using a node to surface contact algorithm. Definition of the card is similar to that defined in the surface to surface contact algorithm of the Lagrangian formulation which requires defining the slave part, the master part and the penalty stiffness. The nodes should be defined as the slave while the shell elements the master. The same penalty stiffness is used as in table 3.3. The LS-DYNA keyword file of the SPH model is attached in appendix D.

### **3.7 INVESTIGATION OF THE EFFECT OF CURVATURE ON IMPACT RESPONSE DUE TO THE BIRD STRIKE**

A simplified finite element model of an aircraft windshield shown in figure 3.7 is modeled. The objective of modeling the windshield is to investigate what effect curvature, of an aircraft windshield, has on the impact response due to bird strike.

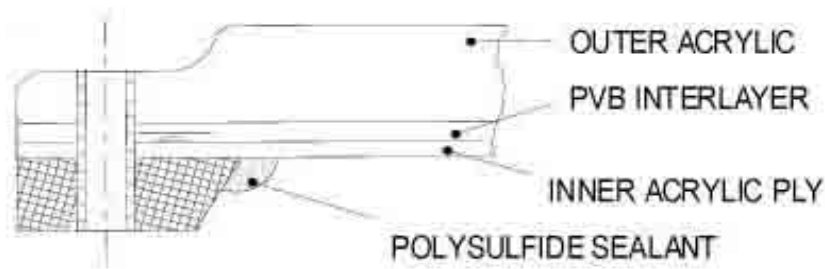


Figure 3.7: Cockpit Window for a Transport Aircraft [22]

The windshield as shown in figure 3.7 is used in the cockpit window for a couple of transport aircraft namely Airbus A318, A319, A320, etc [22]. As seen from the figure, it consists of an acrylic outer ply, Polyvinyl Butyral (PVB) interlayer and an acrylic inner ply.

The exact dimension of the windshield is not known. An initial flat panel of the windshield with the dimension and boundary conditions as shown in figure 3.3 and 3.4 is modeled. The only difference is that the target consists of 3 layers each of 0.002m thick instead of just 1 layer. The properties of the materials used in the manufacture of the aircraft transparency are also not known. Attempts are made to give as realistic a value to the various components as possible. The lack of data does not present a problem since only a relative comparison of the response due to different curvature is desired. The interlayer bond is assumed perfect with no de-bonding or slipping between layers during impact. This preliminary study investigates the response of the transparency of different curvature within the elastic limit of the material. The objective of the study is not to predict actual failure load.

The property of the acrylic layers are defined by card \*MAT\_PLASTIC\_KINEMATIC.

Within the card, the parameters defined are summarized in table 3.5.

Table 3.5: Properties of Acrylic Layer [23]

No.	Properties of Acrylic Layer	Values Chosen
1	Mass Density	1180 kg/m <sup>3</sup>
2	Young's Modulus	3.1 GPa
3	Poisson Ratio	0.4
4	Yield Stress	73.5 MPa
5	Tangent Modulus	0
6	Hardening Parameter	0.5

Properties of PVB interlayer is define by card \*MAT\_VISCOELASTIC. Within the card, the parameters defined are summarized in table 3.6.

Table 3.6: Properties of PVB Layer [21]

No.	Properties of PVB Layer	Values Chosen
1	Mass Density	1100 kg/m <sup>3</sup>
2	Elastic Bulk Modulus	2 GPa
3	Short Time Shear Modulus	1 GPa
4	Long Time Shear Modulus	0.69MPa
5	Decay Constant	12.6 s <sup>-1</sup>

The amount of plate material is kept constant while varying the curvature of the plate as illustrated in figure 3.8. The various introduced curvature are shown in table 3.7 in order of increasing radius of curvature.

Table 3.7: Plate Number and Introduced Curvature

Plate No.	Radius of Curvature
1	0.5m
2	1 m
3	2m
4	4m
5	Infinite (Flat Plate)

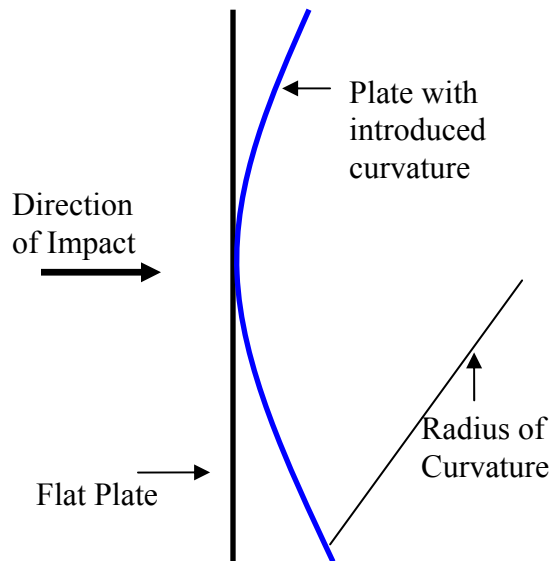


Figure 3.8: Side View of plate and Introduced Curvature

The LS-DYNA keyword file modeling the windshield as discussed is attached in appendix E.

## ***CHAPTER FOUR – RESULTS AND DISCUSSIONS***

### **4.1 EXPECTED RESULT FROMS THE LAGRANGIAN BIRD MODEL**

The verification of the bird parameters as well as the Lagrangian bird model focus on the accurate

- 1) Modeling of pressure profile at the centre of the rigid target during the impact.
- 2) Representation of Hugoniot pressure at the centre of the rigid target.
- 3) Representation of Stagnation pressure at the centre of the rigid target.
- 4) Representation of bird trajectory after the impact.

Figure 4.1 – 4.3 and table 4.1 are the expected numerical results to be obtained from the Lagrangian bird model. They are obtained from a couple of sources. The experimental pressure-time plot at the centre of the rigid target for a 1.82kg bird with an impact velocity of 116m/s is shown in figure 4.1. Table 4.1 summarized the theoretical and experimental Hugoniot and Stagnation pressure. Figure 4.2 – 4.3 shows the bird trajectory obtained from reported numerical studies.

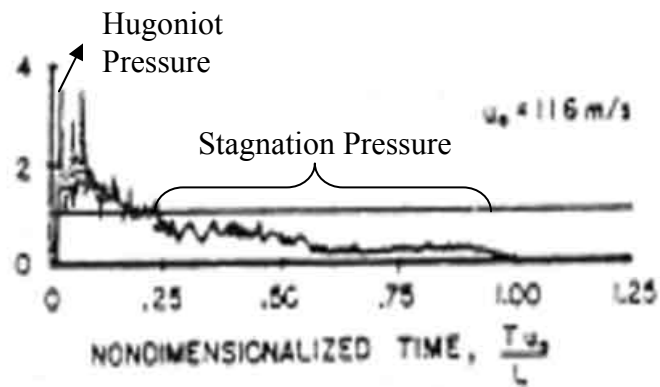


Figure 4.1: Pressure-Time Plot for Bird Impact on Rigid Plate at 116m/s [12]

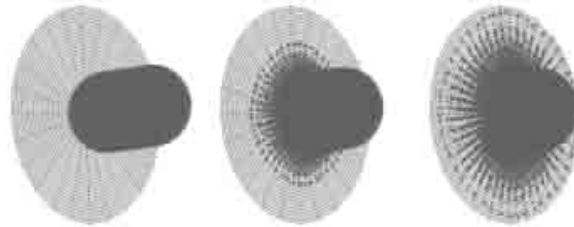


Figure 4.2: Bird Trajectory of a SPH Bird Model after Impact [10]

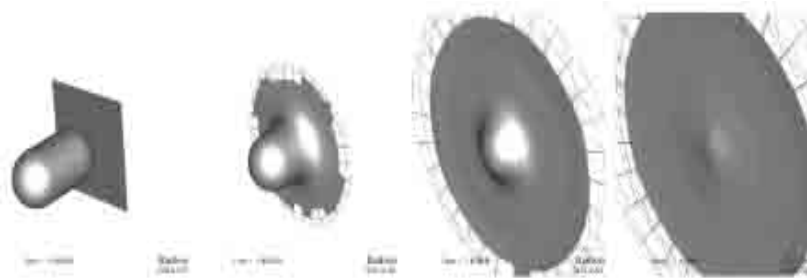


Figure 4.3: Bird Trajectory of a Lagrangian Bird Model after Impact [12]

Table 4.1: Expected Hugoniot and Stagnation Pressure [12]

	Hugoniot Pressure	Stagnation
Theory	100MPa	6MPa
Experimental	60MPa	5MPa

## 4.2 NUMERICAL RESULTS FROM THE LAGRANGIAN BIRD MODEL

Figure 4.4 shows the pressure time plot obtained from the element at the tip of the Lagrangian bird model which is modeled as described in section 3.1, 3.2 and 3.4. Figure 4.5 shows the bird trajectory after impact in the direction that is normal to the plate.

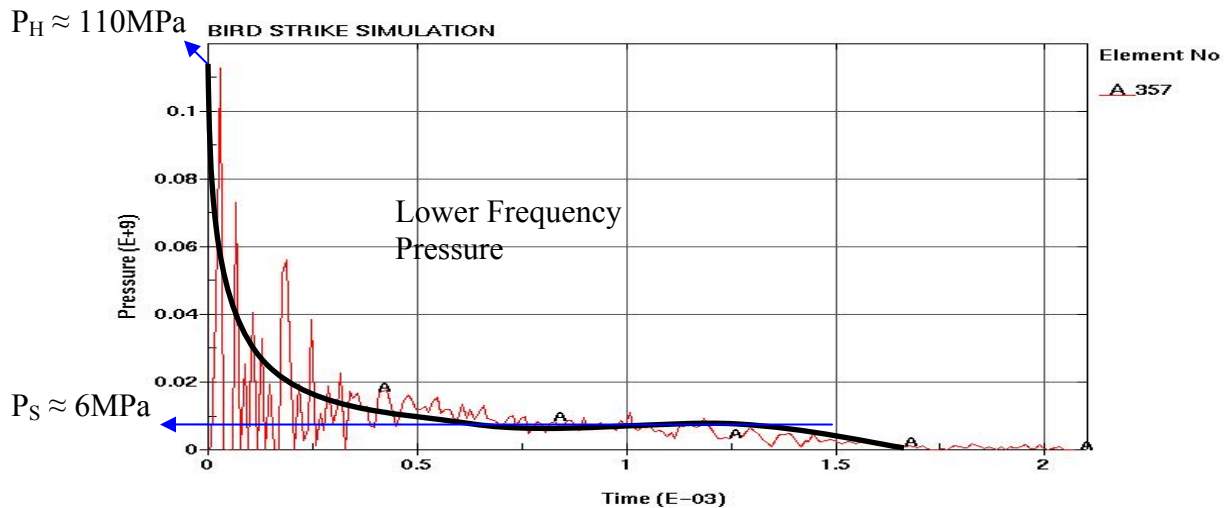


Figure 4.4: Pressure-Time Plot Obtained from the Lagrangian Bird Model

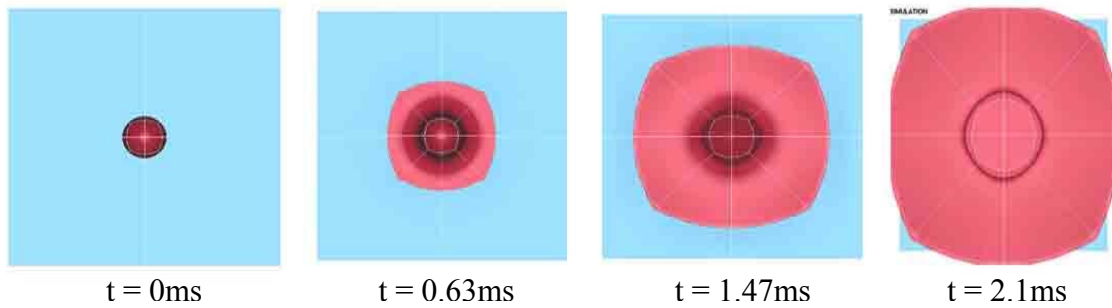


Figure 4.5: Bird Trajectory of Lagrangian Bird Model (In Direction Normal to the Plate)

Referring to figure 4.4, the profile of the pressure time plot predicted by the Lagrangian bird model resembles the experimental plot as shown in figure 4.1. Both plots show a quick rise to the Hugoniot pressure at the initial instant of impact followed by pressure decay and then a period of steady flow pressure known as the stagnation pressure. From figure 4.4, the Hugoniot pressure and stagnation pressure is measured from the graph to be approximately 110MPa and 6MPa respectively. The predicted Hugoniot pressure by the Lagrangian bird model is about 85% higher than the experimental result while the predicted stagnation pressure is 20% higher than the experimental result. The Lagrangian bird model predicted that the bird material will flow on the target in an expanding disc like manner as shown in figure 4.5. This is in conformity with the results of other reported studies as shown by figure 4.2 and 4.3.

A certain degree of conformance could be obtained for the pressure profile, magnitude of stagnation pressure and the bird trajectory. However the difference of 85% between numerical and experimental Hugoniot pressure is too much. The predicted Hugoniot

pressure of 110 MPa is even higher than the theoretical Hugoniot pressure of 100 MPa. Attempts were made to acquire a better conformance between the numerical and experimental Hugoniot pressure.

The Hugoniot pressure could have been exaggerated due to the constant stress elements that are used to model the Lagrangian bird. Constant stress elements are prone to zero energy mode or hourglassing mode which could have affected the numerical result. Figure 4.6 showed the energy plot obtained from the simulation.

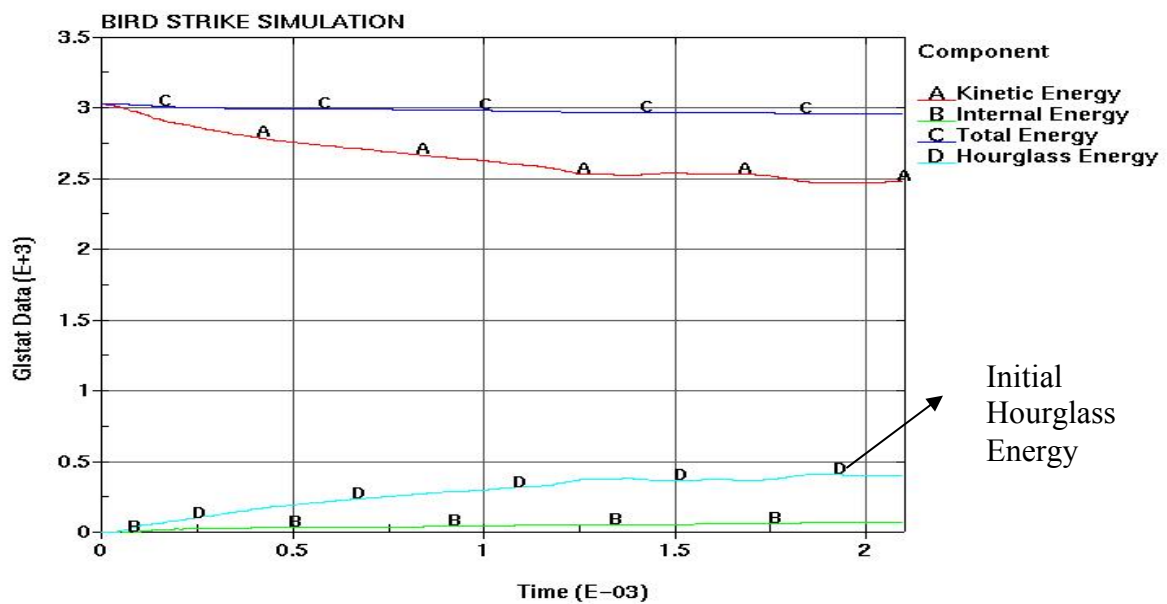
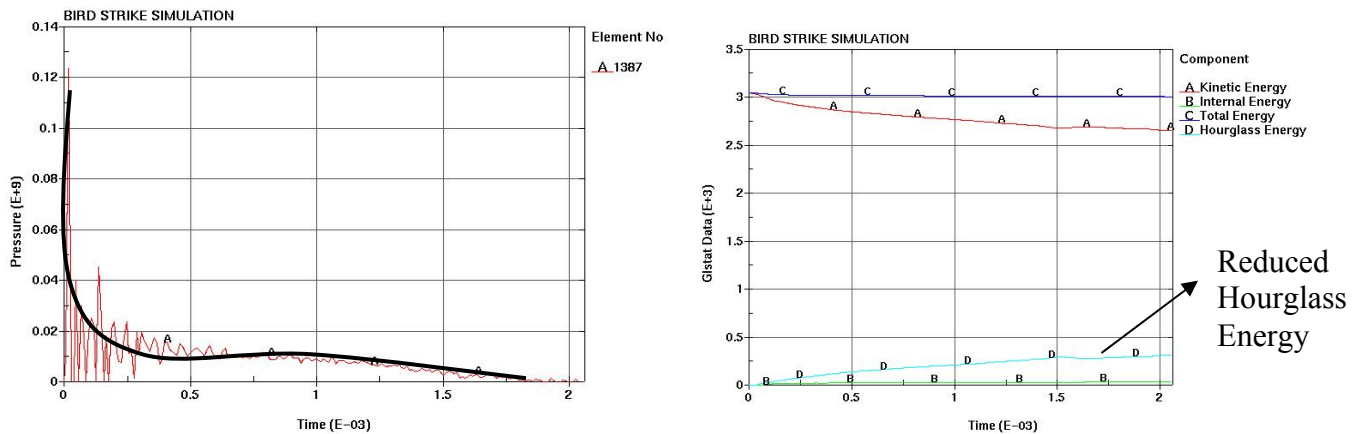


Figure 4.6: Energy Plot (Lagrangian Bird Model)

As seen from figure 4.6, hourglass energy constitutes about 16% of the overall energy. One way of reducing the hourglassing mode is to increase the mesh density of the Lagrangian bird. A quarter Lagrangian bird model with a denser mesh of 2107 elements (about 4 times the mesh density of the initial model) is modeled hoping that by reducing

the hourglass energy, a better approximation of the Hugoniot pressure could be obtained. Figure 4.7 shows the pressure time and energy plot of the Lagrangian bird with the refined mesh. With the higher mesh density, computational time increases about 5 times, from the initial 10 minutes to about an hour. 2 conclusions are made from the plot in figure 4.4, 4.6 and 4.7.



**Figure 4.7: Pressure-Time Plot (Left) and Energy Plot (Right)  
(Lagrangian Bird Model with Higher Mesh Density)**

The pressure profile of figure 4.7 and figure 4.4 looks similar. A higher mesh density does not have a substantial influence on the pressure profile although 5 times more computational time is required. The first conclusion made base on figure 4.4 and 4.7 is that the initial mesh of 525 elements for the quarter bird is sufficient to represent the pressure profile at the centre of the target due to impact. With a higher mesh density, the hourglass energy decreases as predicted. It constitutes about 10% of the total energy as shown on the right of figure 4.7. Despite the reduction in hourglass energy, the Hugoniot pressure remains unacceptably high as shown on the left of figure 4.7. It is concluded that the high magnitude of the Hugoniot pressure predicted by the Lagrangian model is

not due to the effect of the hourglass energy. In fact this can be inferred intuitively since the Hugoniot pressure occurs at the beginning of the impact where hourglass energy had not become significant yet.

In the initial bird model, a scale factor of 0.9 is used for the time step to minimize computational time. Theoretically, a smaller time step gives a better prediction to the numerical result since results from a later stage of time is predicted from results that are closer in time when a smaller time step is used. Figure 4.8 shows the pressure time plot obtained from the Lagrangian model (525 elements) with a scale factor of 0.7 for the time step.

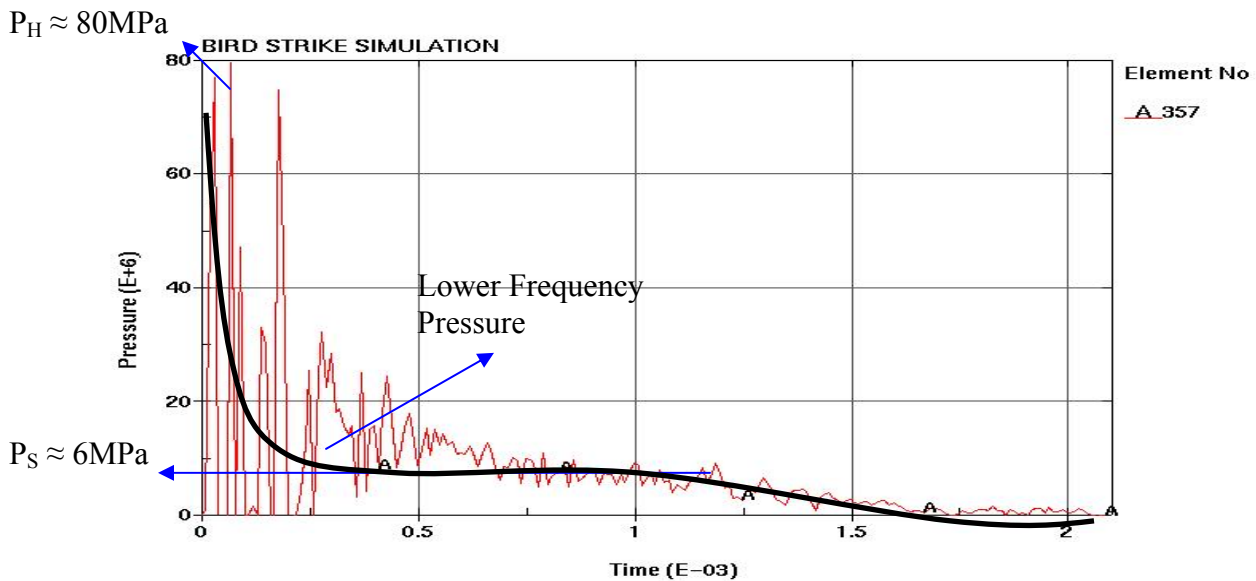


Figure 4.8: Pressure-Time Plot  
(Lagrangian Bird Model with Lower Time Step Scale Factor)

Referring to figure 4.8, with a time step scale factor of 0.7, the Hugoniot pressure is reduced from the original 110 MPa to about 80 MPa. The difference between the

numerical and experimental Hugoniot pressure is approximately 33% compared to the previous 85%. A better agreement between numerical and experimental results is obtained with a lower scale factor. The bird trajectory and the energy plot obtained are similar to figure 4.5 and 4.6.

With a mesh of 525 elements for the quarter bird and a time step scale factor of 0.7, other bird materials are investigated to assess the reliability of the bird material used. The persistent higher Hugoniot pressure compared to experiment might be due to the inadequate bird material used since the pressure distribution on the target is dependent on the constitutive response of the bird model. The parameters of the other bird materials adopted are summarized in table 4.2.

Table 4.2: Parameters of Other Bird Material Used

<b>No.</b>	<b>Description of Bird Material</b>	<b>Constants <math>C_0</math> <math>C_1</math> <math>C_2</math> &amp; <math>C_3</math> of Equation 1</b>
<b>1</b>	Original Bird Material Used (Parameters Obtained from [12])	$C_n = 2250$ MPa for $n = 1$ and 0 otherwise
<b>2</b>	Bird Material with Porosity of 0.1 (Parameters Obtained from Plotting the Curve of Figure 2.4 and Getting the Best Fit Curve. Refer to Appendix F)	$C_0 = 0$ $C_1 = 511.7$ MPa $C_2 = -8224$ MPa $C_3 = 55.15$ GPa
<b>3</b>	Bird Material with Porosity of 0.15 (Parameters Obtained from Plotting the Curve of Figure 2.4 and Getting the Best Fit Curve. Refer to Appendix F)	$C_0 = 0$ $C_1 = 748.4$ MPa $C_2 = -9622.1$ MPa $C_3 = 36.12$ GPa

Figure 4.9 shows the pressure time plot obtained from the Lagrangian bird model with bird material of porosity 0.1 and 0.15. Figure 4.10 shows the pressure time plot of the different bird material plotted on the same graph.

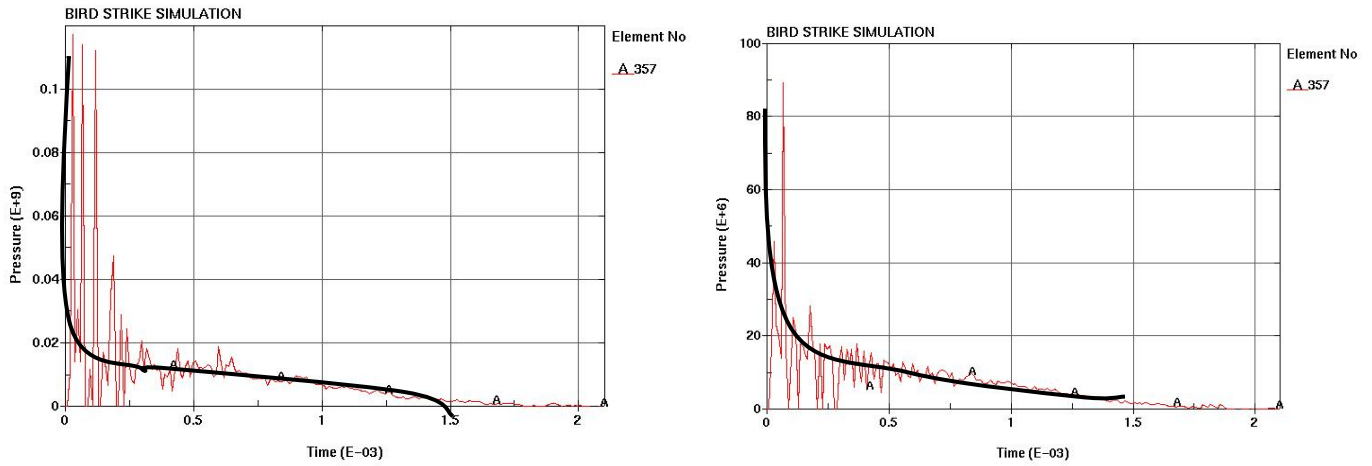


Figure 4.9: Pressure-Time Plot (Lagrangian Bird Model with Different Material Model) (Material of Porosity 0.1(Left), Material of Porosity 0.15 (Right))

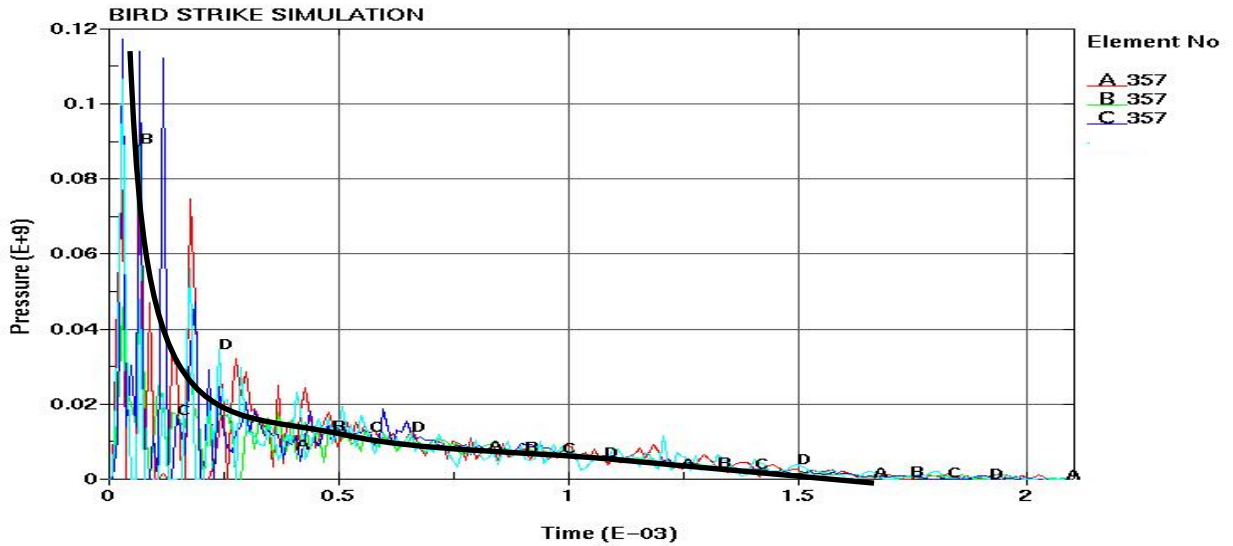


Figure 4.10: Pressure-Time Plot (Lagrangian Bird Model with Different Material Model as Shown in Table 4.3)

Referring to 4.10, the profile of the pressure time plot resembles the one plotted with the original bird material. This shows that all three material models are adequate to a certain extent in representing the pressure distribution on the rigid target due to the impact of the bird. The only significant difference observed from using the different material model is in the Hugoniot pressure. The Hugoniot pressure measured from the pressure time plot of figure 4.9 for the bird material with porosity of 0.1 and 0.15 is approximately 120 MPa and 90MPa respectively, both of which are higher than the Hugoniot pressure predicted by the bird model of the original material. In fact, the original bird material model that is used best represent the pressure measured experimentally from a rigid target due to the impact of a 1.82 kg bird with an impact velocity of 116 m/s.

After refining the Lagrangian bird model and investigating the reliability of the bird material used, a refined Lagrangian bird model with the original bird material, the original mesh density and a time step scale factor of 0.7 is modeled. The final numerical results are summarized in table 4.3. As seen from table 4.3, close resemblance could be obtained for the characteristic of the pressure time plot as well as the bird trajectory after impact. Higher pressure is obtained from the numerical simulation.

Table 4.3: Final Results Obtained from the Lagrangian Bird Model

No.	Verification Parameters	Numerical Results	Comments
1	Characteristic of Pressure Time Plot (Peak, Decay, Steady State)	Figure 4.8	Close resemblance to the experimental plot (Figure 4.1)
2	Hugoniot Pressure	80 MPa	33% difference from experimental result
3	Stagnation Pressure	6 MPa	20% difference from experimental result
4	Bird Trajectory after Impact	Figure 4.5	Trajectory resembles that of an expanding disc. Results similar to those obtained from past reported studies (Figure 4.2 – 4.3)

The higher pressure obtained could be due to the various assumptions made in the numerical model. Using the card \*MAT\_RIGID, the plate is assumed to be perfectly rigid. The boundary of the target is constraint by fixing the degree of freedom of the nodes at the edge of the target in all directions. These two assumptions might be too idealized resulting in the higher numerical pressure obtained. Perfect rigidity is an idealized condition which cannot be realized in real life. In reality, any ‘rigid’ plate deforms to a certain extent on impact. Some of the force is absorbed when the target deforms or give way on impact resulting in the lower experimental pressure obtained. The effect of rigidity on the pressure measured from the target could in fact be observed

from figure 4.13 whereby a deformable target is used instead of a rigid one. As seen from figure 4.13, a lower peak pressure is observed when the target is deformable. This further proves that rigidity of the target does affect the impact response due to bird strike, at least in terms of the pressure measured after the impact. In experimental impact test, the plate would most likely be bolted or clamped. The bolt and clamp might give way due to the high impact force experienced from the impact. By assuming a boundary condition whereby the edges are perfectly constrained is not an accurate representation of the real experiment condition.

The various discrepancies might also be due to the idealization made in the bird model. The shape of the bird is assumed to be a cylindrical with two hemispherical ends. The material property of the bird is assumed to be homogenous and isotropic. In reality, real birds lack homogeneity, isotropy and symmetry. Furthermore, experimental studies are usually accompanied with factors that are beyond control such as the orientation of the bird on impact, the point where the initial impact is etc. Numerical model can never totally predict the experimental result due to the above conditions. A better prediction of the experimental results will usually be accompanied by a corresponding increase in computational cost for the numerical model.

The numerical results obtained from the Lagrangian bird model are overall acceptable. Predicting a higher pressure is more acceptable than predicting a lower pressure since an aircraft that can take higher load is safer than one that can take lower load.

### **4.3 EVALUATION OF THE VARIOUS FINITE ELEMENT FORMULATIONS**

The ALE and SPH bird model are modeled as discussed in section 3.1, 3.3, 3.5 and 3.6. The bird parameters as validated by the Lagrangian bird model are used. Results from the Lagrangian bird serves as a baseline for comparison. The numerical results are obtained from an element at the centre of a deformable aluminum plate modeled using the parameters of table 3.3.

In the assessment on the suitability of the SPH and ALE formulation in modeling bird strike based on the Lagrangian formulation, there are in fact many aspects of numerical results that can be compared against. In this preliminary assessment of the various formulations, the numerical results that are chosen for comparison includes the plot of effective stress, resultant displacement and pressure at the centre of the aluminum plate as well as the energy plot. Other aspects that are compared in this study include the bird trajectory after the impact, the ease of modeling and the computational time required.

Figure 4.11 to 4.13 shows the numerical results obtained from the various formulations. These results are taken for comparison after the respective formulations are compared with a higher mesh density or higher density of particles of their own formulations whereby no significant difference in the results are observed. Refer to Appendix G for the plots of the various formulations.

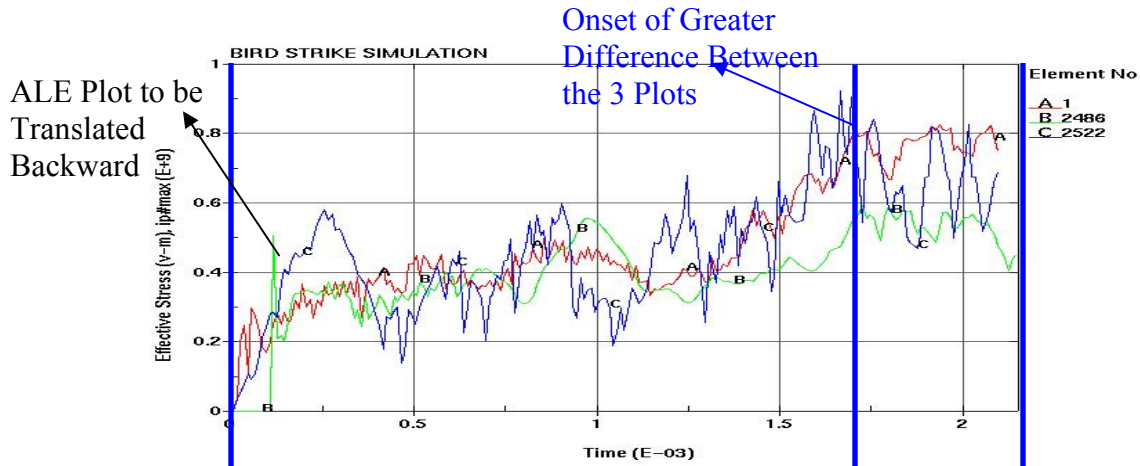


Figure 4.11: Effective Stress Plot  
(A for Lagrangian, B for ALE, C for SPH)

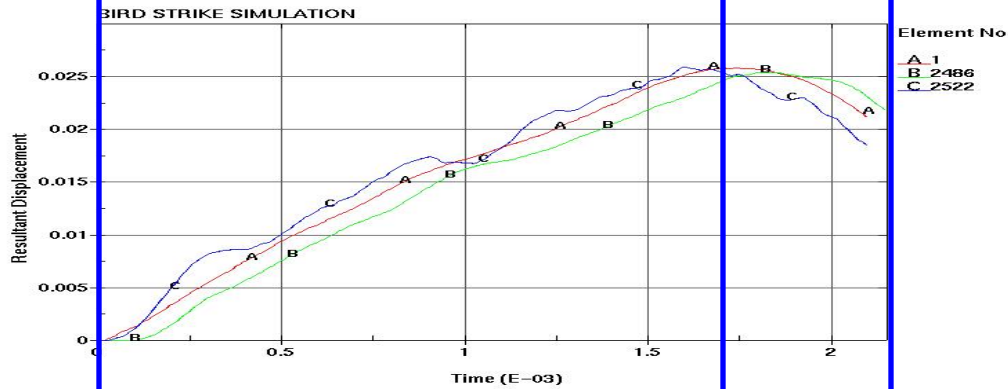


Figure 4.12: Resultant Displacement Plot  
(A for Lagrangian, B for ALE, C for SPH)

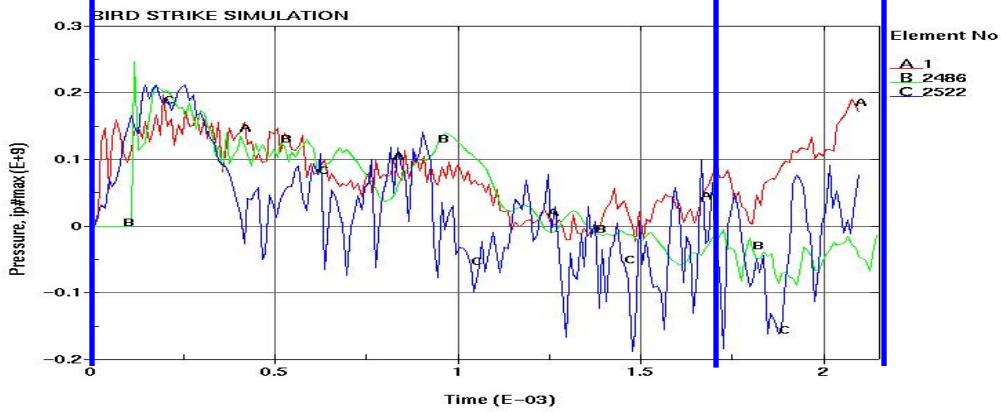


Figure 4.13: Pressure Plot  
(A for Lagrangian, B for ALE, C for SPH)

Referring to figures 4.11 to 4.13, the simulated results for the various formulations show close agreement with one another, at least in terms of the trend showed by the curve of the various formulations. It should be noted that the curve for the ALE formulation should be translated a few milliseconds to the left as the initial time of contact occurs at a later stage compared to the Lagrangian and SPH formulation. This is because the ALE bird is initially position further away from the plate than the SPH and Lagrangian bird model.

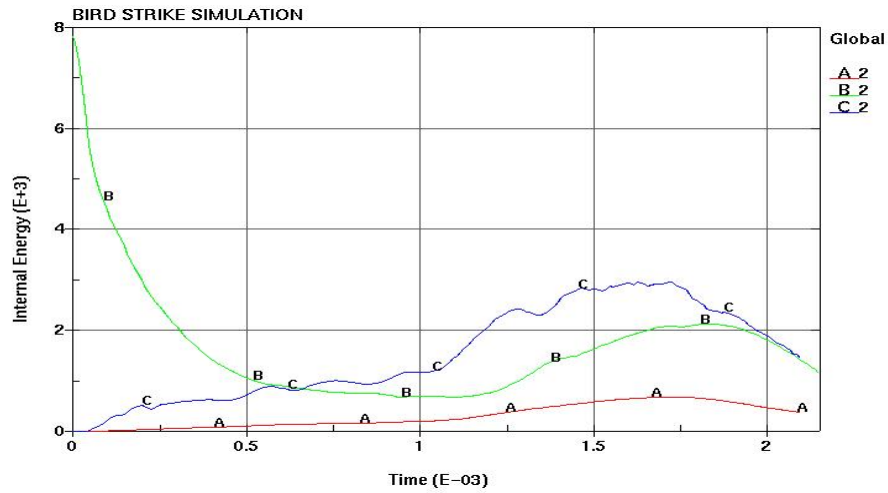
Referring to figure 4.12, the resultant displacement plot has the closest agreement among the three plots compared. All three formulations show an increasing trend in the magnitude of the resultant displacement up to about 1.75 milliseconds whereby it reaches a maximum and then decrease thereafter. All three displacement curve shows approximately similar gradient up till the maximum point. There is a slight difference in gradient for the downward part of the displacement plot which resulted in a difference in the final resultant displacement. The prediction of the 3 different bird model shows less agreement when the elastic plate starts to deform back to its original shape.

Referring to figure 4.11 and 4.13, all 3 formulations predicted the same trend for the effective stress plot and the pressure plot. Similar to the displacement plot, the plots of all 3 formulations showed close conformity up till about 1.75 milliseconds, the onset of greater variation between the 3 plots. The effective stress and pressure plots predicted by the 3 different formulations shows greater disagreement at termination time compared to the resultant displacement plot. This is because effective stress and pressure are both

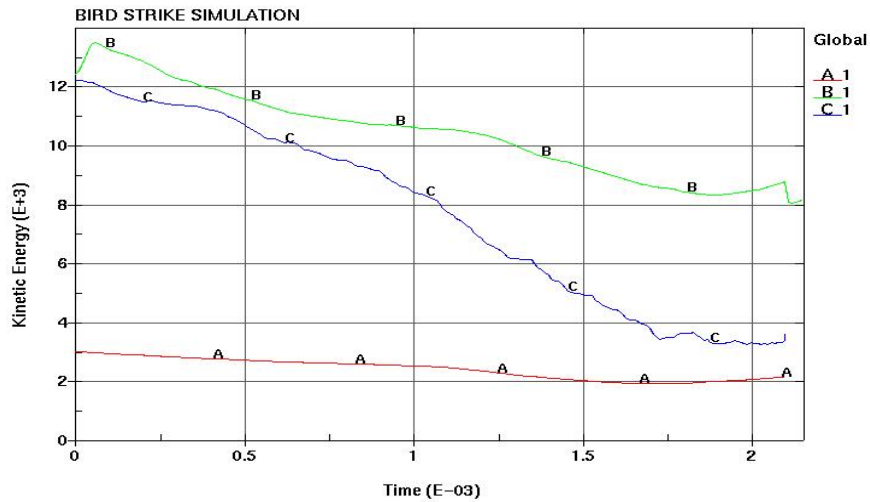
functions of displacement. Since there is a discrepancy in the prediction of displacement, this discrepancy manifest itself in the calculation of effective stress and pressure thus explaining the greater variation at termination time (1.75ms onwards) in the effective stress and pressure plot.

Figure 4.14 to 4.16 shows the energy plot for the various formulations after the impact. Figure 4.14 shows the internal energy plot, figure 4.15 shows the kinetic energy plot and figure 4.16 shows the total energy plot. As observed from figure 4.16, the total energy lost is lowest for the Lagrangian bird model compared to the ALE and SPH bird model. Theoretically the SPH model should give a lower lost in total energy compared to the Lagrangian model as problem such as hourglass energy are not present in SPH model. However this is not the case as observed in figure 4.16. This is probably because a quarter bird is modeled for the Lagrangian model while on the other hand, a full model is modeled for the SPH and ALE bird model. Alternatively, a more proper meshing of the SPH model using a SPH generator as oppose to the unconventional replacement of the element nodes to SPH particles might perhaps results in a lower lost in the total energy. As observed from figure 4.16, there is a sharp drop in the total energy for the ALE model for the first 0.5 milliseconds after which the total energy remains relatively constant. Referring to figure 4.14, the ALE model has a non-zero initial internal energy. This is attributed to the internal energy of the air surrounding the ALE bird model. The initial total energy lost is probably the internal energy of the air surrounding the ALE bird model. All three models show a decrease in kinetic energy after the impact and a corresponding increase in internal energy as observed from figure 4.14 and 4.15.

Referring to figure 4.16 and neglecting the effect of the internal energy of the air for the ALE model, Lagrangian model best conserve energy followed by the ALE model and then the SPH model.



**Figure 4.14: Internal Energy Plot**  
(A for Lagrangian, B for ALE, C for SPH)



**Figure 4.15: Kinetic Energy Plot**  
(A for Lagrangian, B for ALE, C for SPH)

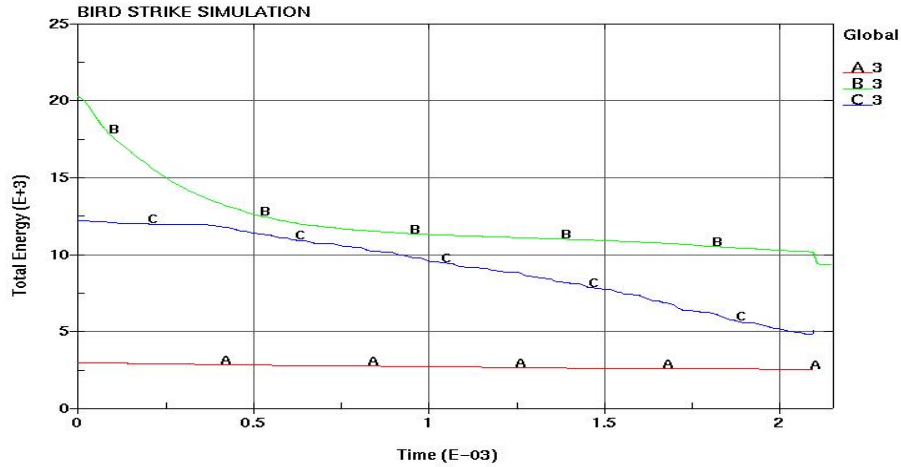


Figure 4.16: Total Energy Plot  
A for Lagrangian, B for ALE, C for SPH)

Figure 4.17 to 4.18 shows the bird trajectory after impact for the SPH and ALE bird model respectively. The bird trajectory after impact for the Lagrangian bird is similar to the one shown in figure 4.5. All 3 models show close resemblance in terms of bird trajectory after impact. It should be noted here however that this applies only if the bird is not split up into parts or debris after impact. If the bird were to split up into debris due to impact on a sharp edge (wing leading edge for example) the Lagrangian formulation might not be able to give an accurate representation of the bird trajectory after impact. In a sense, the ALE and SPH formulation are more versatile as they are more able to represent a wider variety of impact conditions.

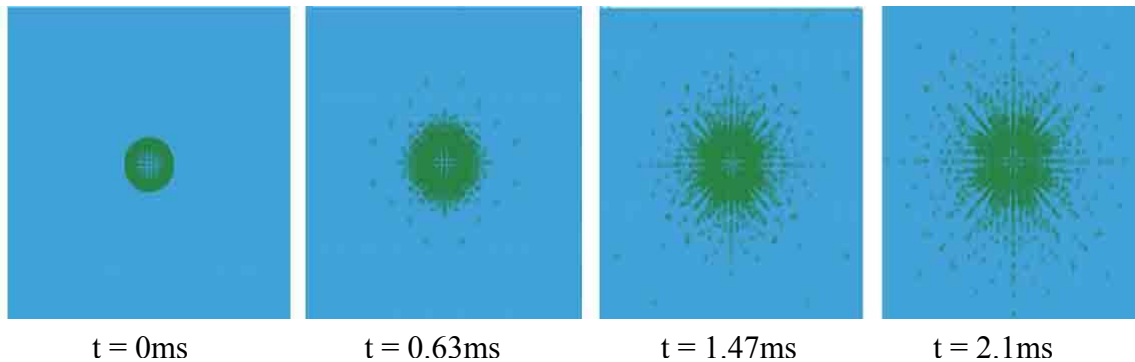


Figure 4.17: Bird Trajectory of SPH Bird Model (In Direction Normal to the Plate)

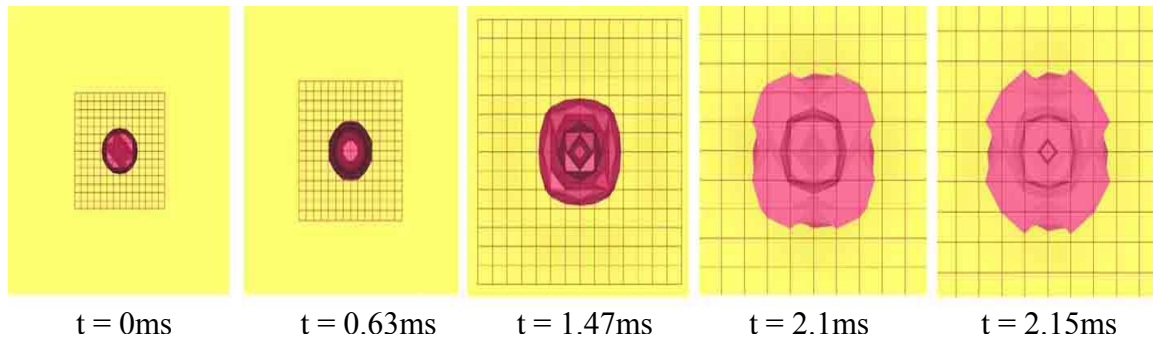


Figure 4.18: Bird Trajectory of ALE Bird Model (In Direction Normal to the Plate)

Comparing the ease of modeling the bird of the various formulations, it is relative easier to model the SPH and the Lagrangian model compared to the ALE model. The SPH and Lagrangian model requires only the definition of the particle's or element's position in space. Modeling of the ALE model requires more effort on the other hand. This is because the ALE model requires the bird material to be contained within the ALE mesh at all time throughout the simulation. The meshing of the ALE model requires some trial and error and it is only through simulation that one is able to know if the mesh had adequately contain the bird material. This trial and error process to ensure the most efficient mesh takes up valuable preprocessing time.

Finally table 4.4 shows the computational time required by the various formulations. This includes formulation base on the higher mesh or particle density as well. To reinstate, the various results compared earlier are based on the bird model with the lower mesh density or particle density.

Table 4.4: Mesh Density and Computational Time for the Various Bird Model

<b>No.</b>	<b>Bird Model</b>	<b>Mesh Density / Number of Nodes</b>	<b>Computational Time</b>
<b>1</b>	Lagrangian Model (Coarse Mesh)	525 elements for a quarter model	5 minutes
<b>2</b>	Lagrangian Model (Denser Mesh)	1568 elements for a quarter model	14 minutes
<b>3</b>	ALE Model (Coarse Mesh)	3528 elements	3 hours 45 minutes
<b>4</b>	ALE Model (Denser Mesh)	10000 elements	6 hours 34 minutes
<b>5</b>	SPH Model (Less Particles)	2662 particles	4 minutes
<b>6</b>	SPH Model (More Particles)	5566 particles	15 minutes

Referring to table 4.4, the ALE bird model takes up much more computational time compared to the Lagrangian and SPH model. With regards to computational time, it is possible to model a quarter Lagrangian or SPH bird model but not a quarter ALE bird model. This is because it is not possible to apply a boundary condition to the bird material within the ALE mesh. The SPH and Lagrangian model is therefore comparatively more efficient in terms of computational time.

The numerical results as shown in this section show close resemblance between the 3 formulations. Therefore it can be concluded that other than using the classical approach in simulation of bird strike, alternatives like the ALE and SPH model can be used as well.

Various advantages and disadvantages pertaining to the different formulations are discussed in this section. It should be noted however the advantages and disadvantages discussed is dependent on the degree of proficiency and understanding of the different formulations by different individuals.

#### **4.4 EFFECT OF CURVATURE ON IMPACT RESPONSE**

The impact response of the various layers of the transparency namely the acrylic outer and inner layer and the PVB middle layer as discussed in section 3.7 is investigated in terms of effective stress. The effect of an increase in curvature of the transparency is next investigated.

Figure 4.19 shows the effective stress of the various layers of a transparency with zero curvature due to the impact, predicted by the Lagrangian bird model.

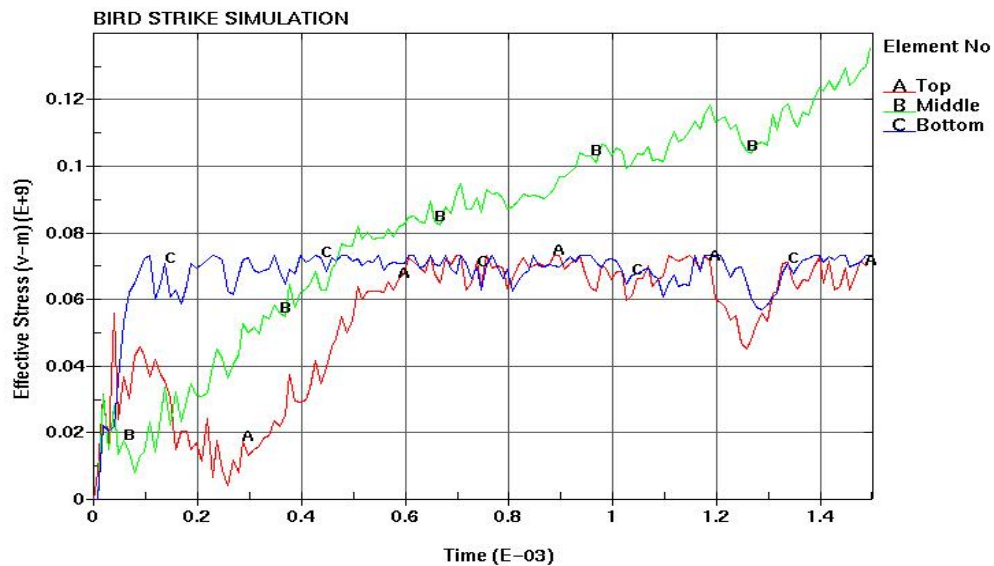


**Figure 4.19: Impact Response of Transparency with no Curvature (A for Outer layer, B for Middle Layer, C for Inner Layer)**

As seen from figure 4.19, all 3 layers experienced a sharp rise of different magnitude in the effective stress due to the initial shock at impact. The PVB layer showed by the green line attains a lower initial peak compared to the acrylic layers. This is probably due to the lower stiffness of PVB compared to acrylic. The acrylic layers each reach a maximum effective stress value after a certain amount of time which signifies that the yield point of the acrylic layer is most probably reached. The inner acrylic layer represented by the blue line reaches maximum effective stress at the initial shock while the outer acrylic layer at a later stage of time. This is probably because tensile stress experienced by the inner acrylic layer is more significant compared to the compressive stress experienced by the outer acrylic layer.

Comparing the effective stress of the different layers due to a difference in the curvature, figure 4.20 to 4.22 shows the effective stress experienced at the outer, middle and inner layer respectively, as a result of a difference of curvature. As observed from figure 4.20 to 4.22, the finite element model predicted that a curved transparency experienced a higher magnitude of effective stress at the initial point of impact. This is due to the higher stiffness of a curved transparency as compared to a flat transparency. Referring to figure 4.20, the finite element model predicted that for the outer acrylic layer, the one with a curvature experienced a higher effective stress for the first 0.4ms compared to the one with infinite radius of curvature. After the first 0.4ms, no significant difference could be observed between the 2 plots as the effective stress tends towards yield stress. The finite element model predicted a higher effective stress experienced at the middle PVB layer by the flat transparency compared to the curved transparency some times after the initial

contact. The difference in effective stress becomes more significant after 0.4ms as observed from figure 4.21. Finally for the inner acrylic layer, finite element model predicted no significant difference in the effective stress experienced for either a curved or flat transparency some times after the initial contact.

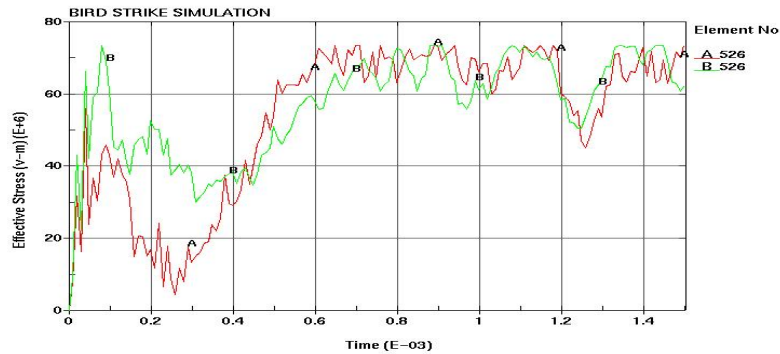


Figure 4.20: Impact Response of Outer Layer of Transparency (A for Flat Target, B for Target with 0.5m Radius of Curvature)

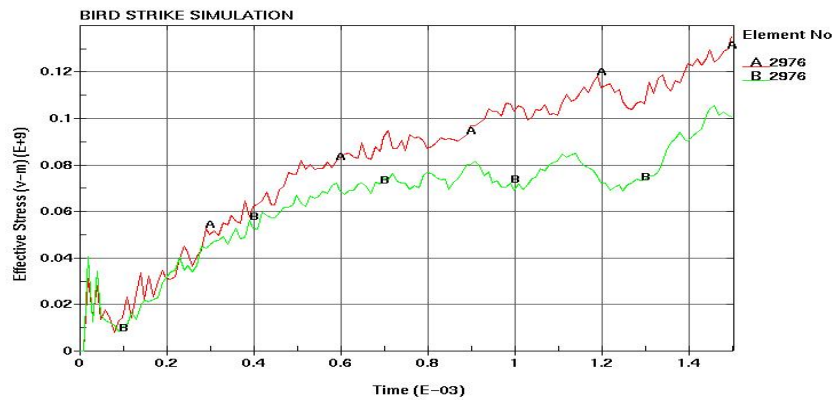


Figure 4.21: Impact Response of Middle Layer of Transparency (A for Flat Target, B for Target with 0.5m Radius of Curvature)

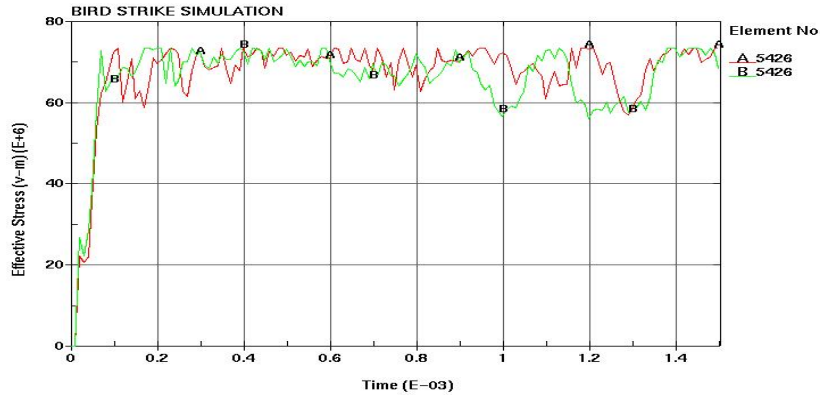


Figure 4.22: Impact Response of Inner Layer of Transparency (A for Flat Target, B for Target with 0.5m Radius of Curvature)

Looking at the effect of an increase in curvature, it can be concluded from the above discussion that an increase in curvature cause an increase in effective stress experienced by all layers at the initial point of contact. After the initial contact, there is an increase in effective stress experienced by the acrylic outer layer while a decrease in effective stress experienced by the PVB middle layer. Due to the sharp rise to yield point at the initial point of impact, the effective stress experienced by the inner acrylic layer after the initial contact is not much affected by the presence of curvature

The effective stress of transparencies with intermediate curvature, (between infinity to 0.5m radius of curvature) as shown in table 3.7 is plotted and attached in appendix H. Generally the gradual increasing or decreasing trend of the effective stress can be observed from the plots attached in the appendix.

## ***CHAPTER FIVE – CONCLUSIONS & RECOMMENDATIONS***

### **5.1 CONCLUSIONS AND RECOMMENDATIONS**

The results obtained from the simulation of the impact of the Lagrangian bird model on a rigid target showed that results obtained from numerical simulation is comparable to experimental one in terms of pressure profile, Hugoniot and stagnation pressure. Both Hugoniot and stagnation pressure obtained are higher than the experimental results which might be attributed to the various assumptions made in modeling the numerical model.

Simulation of bird impact on an elastic aluminum flat panel using different formulations namely Lagrangian, ALE and SPH yields comparable numerical results. The ALE and SPH method provides alternatives to the Lagrangian formulation for the simulation of bird strike. The pros and cons of using the various formulations have been briefly discussed in this report. Depending on the requirement, different formulations can be used under different circumstances so as to achieve the most effective outcome. However the effectiveness and efficiency of using the various formulations depends on the proficiency of individual as discussed earlier.

The effect of curvature, of an aircraft transparency, on the impact response due to bird strike has been investigated. However there is a lack of experimental result to validate the numerical result.

The numerical study of bird strike has been a much studied topic. Large amount of money can be saved in the validation of aircraft components with numerical simulations before the actual testing. This final year project focus on simplified models as the exact geometrical shape and material properties of the various aircraft components are usually not readily available in literature. If more information is available, a more realistic model of the aircraft component could be modeled. This includes a more realistic geometric shape or material model that better represents the aircraft. With a more realistic model, more areas of investigation regarding bird strike can be look into. For example, numerical results can be used to determine the different composition of the aircraft material that achieves the greatest strength with the least amount of material.

## ***APPENDIX A – GENERAL WEIGHT OF SOME SPECIES OF BIRDS***

Table A1: Weight of Some North American Gull Species

<b>Bird Species</b>	<b>Weight (lbs)</b>
Great Black-backed Gull	2.3-5.0
Glaucous Gull	2.4-4.0
Herring Gull	1.6-3.3
Ring-billed Gull	0.83-1.4
Iceland Gull	1.9

Table A2: Weight of Some North American Water Fowl Species

<b>Bird Species</b>	<b>Weight (lbs)</b>
American White Pelican	9.9-30
Mute Swan	3.2-16.5
Tundra Swan	14-21
Canada Goose (the "maxima" race)*	11.0-16+
Canada Goose (the "interior" race)*	6.8-10.4
Canada Goose (the "Canadensis" race)*	7.3-13.8
Snow Goose	5.1-6.6
Brant	1.9-4.0
American Black Duck	1.6-3.5
Mallard	1.2-3.8
Northern Pintail	1.3-2.4
Gadwall	1.4-2.3

Table A3: Weight of Some North American Raptor Species

<b>Bird Species</b>	<b>Weight (lbs)</b>
Bald Eagle	9.1-11.8
Gyr Falcon	2.1-4.4
Turkey Vulture	2.5-3.5
Red-tailed Hawk	2.3-2.7
Rough-legged Hawk	1.7-2.7
Peregrine Falcon	1.4-2.1
Northern Harrier	0.65-1.66
Broad-winged Hawk	0.93-1.1
American Kestrel	0.24-0.26

Above Information obtained from [4]

## APPENDIX B – KEYWORD FILE OF THE LAGRANGIAN BIRD MODEL

```

*KEYWORD
*TITLE
bird strike simulation
*CONTROL_TERMINATION
  0.002100      0      0.0      0.0      0.0
*CONTROL_TIMESTEP
  0.0 0.900000      0      0.0      0.0      0      1
  0.0
*CONTROL_HOURLASS
4
*CONTROL_ENERGY
2
*DATABASE_GLSTAT
1.000e-05
*DATABASE_BINARY_D3PLOT
1.000e-05
*DATABASE_MATSUM
1.0 e-5
*CONTACT_AUTOMATIC_SURFACE_TO_SURFACE_TITLE
$#      cid      title
$#      1
$#      ssid      msid      sstyp      mstyp      sboxid      mboxid      spr      mpr
$#      1      2      3      3      0      0      1      1
$#      fs      fd      dc      vc      vdc      penchk      bt      dt
$#      0.0      0.0      0.0      0.0      0.0      0      0.0      0.0
$#      sfs      sfm      sst      mst      sfst      sfmt      fsf      vsf
$#      26.5150  1.000000      0.0      0.0      0.0      0.0      0.0      0.0
$#      soft      sofscl      lcidab      maxpar      sbopt      depth      bsort      frcfrq
$#      0      0.0      0      0.0      0.0
*PART
1 1 1 1 → Part 1 defines the bird
*SECTION_SOLID
1 1
*MAT_NULL
1 938.5000      0 0.001000      0.0      0.0      0.0      0.0
$*EOS_LINEAR_POLYNOMIAL
$ 1 0 511.70e6 -8224.4e6 55.15e9 0.0 0.0 $0.0
$ 0.0
$*EOS_LINEAR_POLYNOMIAL
$ 1 0 748.40e6 -9622.1e6 36.12e9
$
*EOS_LINEAR_POLYNOMIAL
1 0 2250e6
*PART
2 2 2
*SECTION_SHELL
2 0 → Part 2 defines the target
$*MAT_RIGID_TITLE
$Target
$ 2 2700.00007.0000e+10 0.300000 0.0 0.0 0.0 $
$
$
*MAT_ELASTIC
2 2700.00007.0000e+10 0.300000 0.0 0.0 0.0
1 2 0.0 116.00000 0.0 0.0
0.0 0.0 0.0 0.0
Material definition card for the rigid
and elastic plate respectively

```

```
$
$ NODES
$
*NODE
1,-0.114000000,0.000000000E+00,0.000000000E+00,5,7
2,-0.113009997,0.000000000E+00,1.057733782E-02,2,6
3,-0.110074371,0.000000000E+00,2.078727446E-02,2,6
...
...
$
$ ELEMENT CARDS FOR SOLID ELEMENTS
$
*ELEMENT_SOLID
1,1,1,37,43,7,2,38,44,8
2,1,37,73,79,43,38,74,80,44
3,1,7,43,49,13,8,44,50,14
...
...
$
$ ELEMENT CARDS FOR SHELL ELEMENTS
$
*ELEMENT_SHELL_THICKNESS
1,2,793,829,830,794
0.100000E-01,0.100000E-01,0.100000E-01,0.100000E-01
2,2,829,865,866,830
0.100000E-01,0.100000E-01,0.100000E-01,0.100000E-01
3,2,865,901,902,866
0.100000E-01,0.100000E-01,0.100000E-01,0.100000E-01
...
...
*END
```

## APPENDIX C – KEYWORD FILE OF THE ALE BIRD MODEL

```

*KEYWORD
*TITLE
bird strike simulation
*ALE_REFERENCE_SYSTEM_GROUP
1,1,4,0,0,0,0

*DATABASE_MATSUM
1.0e-5
*CONTROL_TERMINATION
0.00215
*CONTROL_TIMESTEP
0.0, 0.9
*DATABASE_BINARY_D3PLOT
1.0e-5
*DATABASE_GLSTAT
1.0e-5
*CONTROL_ALE
0, 1, 2, -1.0

*ALE_MULTI-MATERIAL_GROUP
1, 1
3, 1
*CONSTRAINED_LAGRANGE_IN_SOLID
4,1,1,1,4,4,2,1

*MAT_NULL
1,1.225,0,0
*MAT_NULL
3,938.5,0,0.001
*EOS_LINEAR_POLYNOMIAL
3,0,2250e6

*EOS_LINEAR_POLYNOMIAL
1,0,0,0,0,0.4,0.4,0
250000,1
*MAT_ELASTIC
2,8000,200.0E9,0.3
*MAT_ELASTIC
4 2700.00007.0000e+10 0.300000 0.0 0.0 0.0

*SECTION_SOLID
1, 11
*SECTION_SOLID
3, 11
*SECTION_SHELL
2, 0

*SECTION_SHELL
4, 0

*PART
1, 1, 1, 1 → Part 1 defines the bird
*PART
2, 2, 2 → Part 2 defines the shell containing the bird material
*PART
3, 3, 3, 3 → Part 3 defines the air surrounding the bird

*PART
4, 4, 4 → Part 4 defines the target
*INITIAL_VOLUME_FRACTION_GEOMETRY
1, 1, 1

```

```

1, 0, 2
2, 1, 0
*INITIAL_VELOCITY_GENERATION
1, 2, 0.0, 116.0

*LOAD_SEGMENT_SET
1,1,1,0
*LOAD_SEGMENT_SET
2,1,1,0
*LOAD_SEGMENT_SET
3,1,1,0
*LOAD_SEGMENT_SET
4,1,1,0
*LOAD_SEGMENT_SET
5,1,1,0
*LOAD_SEGMENT_SET
6,1,1,0
*DEFINE_CURVE
1
0.000,0.0
0.00001,100000.0
0.0021,100000.0
$
$ NODES
$
*NODE
1,0.129999995,-0.349999994,-0.349999994,7,7
2,0.129999995,-0.349999994,-0.340000004,7,7
3,0.129999995,-0.349999994,-0.329999983,7,7
...
...
$
$ ELEMENT CARDS FOR SOLID ELEMENTS
$
*ELEMENT_SOLID
1,1,6250,6475,6490,6265,6251,6476,6491,6266
2,1,6475,6700,6715,6490,6476,6701,6716,6491
3,1,6700,6925,6940,6715,6701,6926,6941,6716
...
...
$
$ ELEMENT CARDS FOR SHELL ELEMENTS
$
*ELEMENT_SHELL_THICKNESS
1,4,72,1,2,73
0.100000E-01,0.100000E-01,0.100000E-01
2,4,143,72,73,144
0.100000E-01,0.100000E-01,0.100000E-01,0.100000E-01
3,4,214,143,144,215
0.100000E-01,0.100000E-01,0.100000E-01,0.100000E-01
...
...
$
$ Face set face1
$
*SET_SEGMENT
1,0.000E+00,0.000E+00,0.000E+00,0.000E+00
6489,6264,6279,6504,0.000E+00,0.000E+00,0.000E+00,0.000E+00
6714,6489,6504,6729,0.000E+00,0.000E+00,0.000E+00,0.000E+00
...
...
$
$ Face set face2
$
*SET_SEGMENT
2,0.000E+00,0.000E+00,0.000E+00,0.000E+00
10990,10975,10976,10991,0.000E+00,0.000E+00,0.000E+00,0.000E+00

```

```
11005,10990,10991,11006,0.000E+00,0.000E+00,0.000E+00,0.000E+00
...
...
...
$
$ Face set face3
$
*SET_SEGMENT
3,0.000E+00,0.000E+00,0.000E+00,0.000E+00
6250,6475,6490,6265,0.000E+00,0.000E+00,0.000E+00,0.000E+00
6475,6700,6715,6490,0.000E+00,0.000E+00,0.000E+00,0.000E+00
...
...
...
$
$ Face set face4
$
*SET_SEGMENT
4,0.000E+00,0.000E+00,0.000E+00,0.000E+00
6250,6265,6266,6251,0.000E+00,0.000E+00,0.000E+00,0.000E+00
6265,6280,6281,6266,0.000E+00,0.000E+00,0.000E+00,0.000E+00
...
...
...
$
$ Face set face5
$
*SET_SEGMENT
5,0.000E+00,0.000E+00,0.000E+00,0.000E+00
6461,6460,6685,6686,0.000E+00,0.000E+00,0.000E+00,0.000E+00
6911,6910,7135,7136,0.000E+00,0.000E+00,0.000E+00,0.000E+00
...
...
...
$
$ Face set face6
$
*SET_SEGMENT
6,0.000E+00,0.000E+00,0.000E+00,0.000E+00
6250,6251,6476,6475,0.000E+00,0.000E+00,0.000E+00,0.000E+00
6475,6476,6701,6700,0.000E+00,0.000E+00,0.000E+00,0.000E+00
...
...
*END
```

## APPENDIX D – KEYWORD FILE OF THE SPH BIRD MODEL

```

*KEYWORD
*TITLE
LS-DYNA keyword deck by LS-PRE
*CONTROL_SPH
    1          11.0000e+20          0          500          0          0.01.0000e+15
*CONTROL_TERMINATION
    0.002100          0          0.0          0.0          0.0
*CONTROL_CONTACT
0, 0, 0, 2, 2

*CONTROL_HOURLASS
4

*DATABASE_BINARY_D3PLOT
1e-5
*DATABASE_GLSTAT
1e-4
*CONTROL_ENERGY
2
*CONTACT_CONSTRAINT_NODES_TO_SURFACE
$#      ssid      msid      sstyp      mstyp      sboxid      mboxid      spr      mpr
$#      fs        fd        dc        vc        vdc        penchk      bt        dt
$#      sfs       sfm       sst       mst       sfst       sfmt       fsf       vsf
    26.515       1.0       0.0       0.0       1.000000   1.000000   1.000000   1.000000

*PART
    1          1          1          1          1
*SECTION_SPH
    1  1.200000  0.200000  2.000000          0.01.0000e+20          0.0
*MAT_NULL
    1  938.50000          0.0  0.001000          0.0          0.0          0.0          0.0
*EOS_LINEAR_POLYNOMIAL
    1          0.02.2500e+09          0.0          0.0          0.0          0.0          0.0
    0.0          0.0

*PART
    2          2          2
*SECTION_SHELL
    2          2  1.000000          2          1          0.0          0          1
    0.1          0.1          0.1          0.1          0          0.0
*MAT_ELASTIC
    2  2700.00007.0000e+10  0.300000          0.0          0.0          0.0
*INITIAL_VELOCITY_NODE
    1  116.00000          0.0          0.0          0.0          0.0          0.0
    2  116.00000          0.0          0.0          0.0          0.0          0.0
    3  116.00000          0.0          0.0          0.0          0.0          0.0
...
...
...
*DEFINE_BOX
    1 -0.114000  0.121000 -0.350000  0.350000 -0.350000  0.350000
*ELEMENT_SHELL_THICKNESS
$
$ ELEMENT CARDS FOR SHELL ELEMENTS
$
    1          2      2663      2735      2736      2664
    0.01000000      0.01000000      0.01000000      0.01000000
    2          2      2735      2807      2808      2736
    0.01000000      0.01000000      0.01000000      0.01000000
    3          2      2807      2879      2880      2808
    0.01000000      0.01000000      0.01000000      0.01000000

```

```
...
...
...
*ELEMENT_SPH
    1      1      6.837e-4
    2      1      6.837e-4
    3      1      6.837e-4
...
...
...
*NODE
$
$ NODES
$
    1      -0.08344734      -0.03570391      -0.03570391
    2      -0.08607367      -0.03924946      -0.02938028
    3      -0.08816797      -0.04207675      -0.02251898
...
...
...
*SET_NODE_LIST
1,0.,0.,0.,0.
1,122,243,364,485,606,727,848
969,1090,1211,1332,1453,1574,1695,1816
1937,2058,2179,2300,2421,2542,12,133
...
...
...
*END
```

## *APPENDIX E – KEYWORD FILE OF THE AIRCRAFT WINDSHIELD*

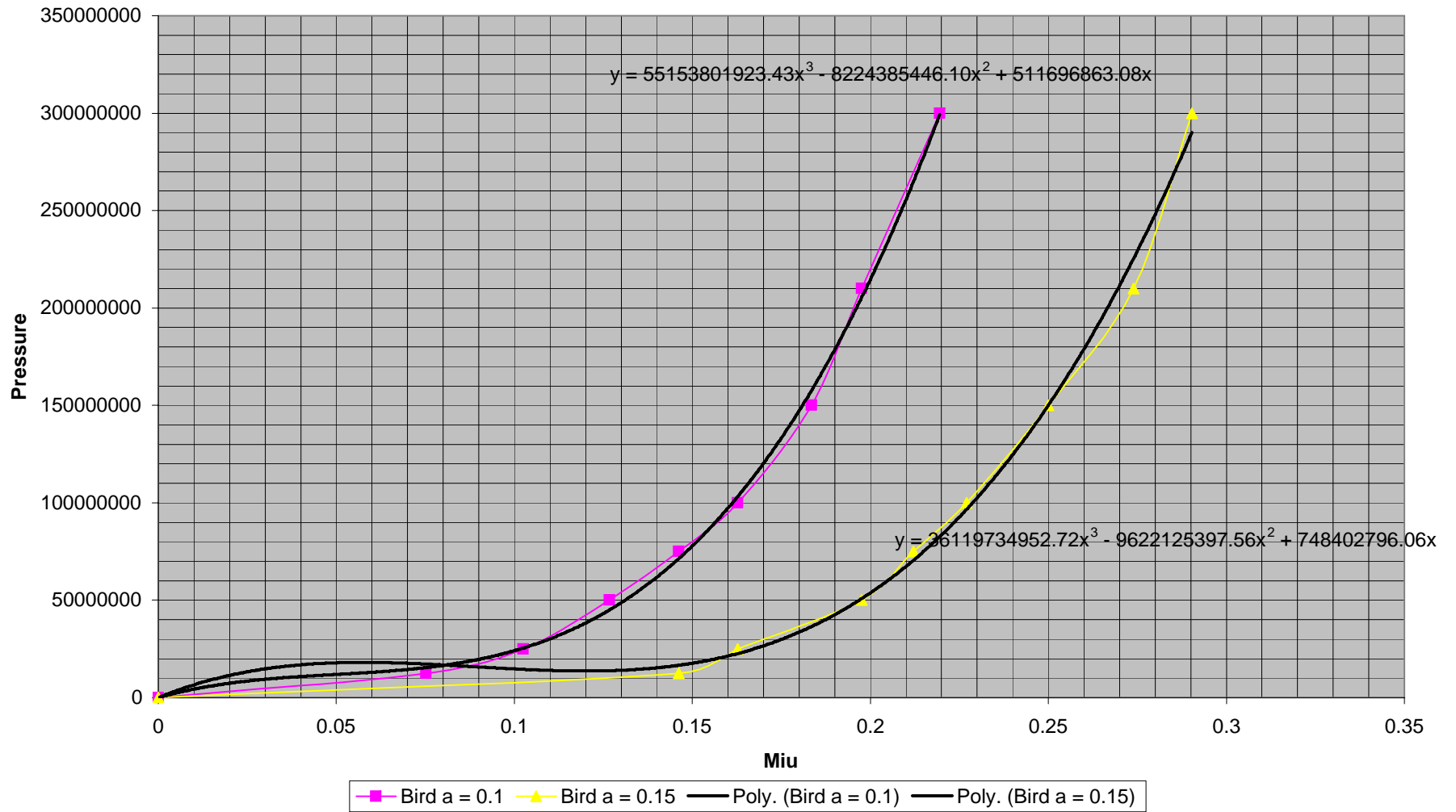
```

*KEYWORD
*TITLE
bird strike simulation
*CONTROL_TERMINATION
0.001500 0 0.0 0.0 0.0
*CONTROL_TIMESTEP
0.0 0.900000 0 0.0 0.0 0 1
0.0
*CONTROL_HOURLASS
4
*CONTROL_ENERGY
2
*DATABASE_GLSTAT
1.000e-05
*DATABASE_BINARY_D3PLOT
1.000e-05
*DATABASE_MATSUM
1.0 e-5
*CONTACT_AUTOMATIC_SURFACE_TO_SURFACE_TITLE
$# cid title
1
$# ssid msid sstyp mstyp sboxid mboxid spr mpr
1 2 3 3 0 0 1 1
$# fs fd dc vc vdc penchk bt dt
0.0 0.0 0.0 0.0 0.0 0 0.0 0.0
$# sfs sfm sst mst sfst sfmt fsf vsf
2.34900 1.000000 0.0 0.0 0.0 0.0 0.0 0.0
$# soft sofsc1 lcidab maxpar sbopt depth bsort frcfreq
0 0.0 0 0.0 0.0
*PART
1 1 1 1 → Part 1 defines the bird
*SECTION_SOLID
1 1
*MAT_NULL
1 938.5000 0 0.001000 0.0 0.0 0.0 0.0
*EOS_LINEAR_POLYNOMIAL
1 0 2250e6
*INITIAL_VELOCITY_GENERATION
1 2 0.0 116.00000 0.0 0.0
0.0 0.0 0.0 0.0 0.0 0.0
*PART
2 2 2 → Part 2 defines the acrylic outer layer
*SECTION_SOLID
2 1 1
*PART
4 4 4 → Part 4 defines the acrylic inner layer
*SECTION_SOLID
4 1 1
*MAT_PLASTIC_KINEMATIC
2 1180.00003.1000e+09 0.4000007.3500e+07 0.0 0.500000
0.0 0.0 0.0 0.0
*MAT_PLASTIC_KINEMATIC
4 1180.00003.1000e+09 0.4000007.3500e+07 0.0 0.500000
0.0 0.0 0.0 0.0
*PART
3 3 3 → Part 3 defines the PVB middle layer
*SECTION_SOLID
3 1 1
*MAT_VISCOELASTIC

```

```
3 1100.00002.0000e+091.0000e+096.9000e+05 12.600000
$
$ NODES
$
*NODE
1,0.115000010,0.000000000E+00,0.000000000E+00,5,7
2,0.115045860,0.000000000E+00,9.557154030E-03,2,6
3,0.115183055,0.000000000E+00,1.911343262E-02,2,6
...
...
$
$ ELEMENT CARDS FOR SOLID ELEMENTS
$
*ELEMENT_SOLID
1,2,1,1297,1333,37,2,1298,1334,38
2,2,1297,2593,2629,1333,1298,2594,2630,1334
3,2,37,1333,1369,73,38,1334,1370,74
...
...
*END
```

### APPENDIX F: CHART OF PRESSURE AGAINST MIU



## ***APPENDIX G – DIFFERENT FORMULATIONS OF DIFFERENT MESH/ PARTICLES DENSITY***

2 models are modeled for each formulation. One has a higher mesh or particle density while the other has a lower mesh or particle density. The relevant information is summarized in table G1.

Table G1: Mesh Density and Computational Time for the Various Bird Model

No.	Bird Model	Mesh Density / Number of Nodes	Computational Time
1	Lagrangian Model (Coarse Mesh)	525 elements for a quarter model	5 minutes
2	Lagrangian Model (Denser Mesh)	1568 elements for a quarter model	14 minutes
3	ALE Moel (Coarse Mesh)	3528 elements	3 hours 45 minutes
4	ALE Model (Coarse Mesh)	10000 elements	6 hours 34 minutes
5	SPH Model (Less Particles)	2662 particles	4 minutes
6	SPH Model (More Particles)	5566 particles	15 minutes

Figure G1 to G3 shows the plot of effective stress, resultant displacement and pressure for the 2 models of different mesh density of the Lagrangian bird model. Figure G4 to G6 shows the plots for the ALE model. Figure G7 to G9 shows the plots for the SPH model.

Basically the various plots pertaining to each formulation show great resemblance to one another. The results of this mesh sensitivity study indicate that the relatively coarse models are sufficient to give a comparable result to the other formulations. Generally, the more nodes there are the longer the computational time.

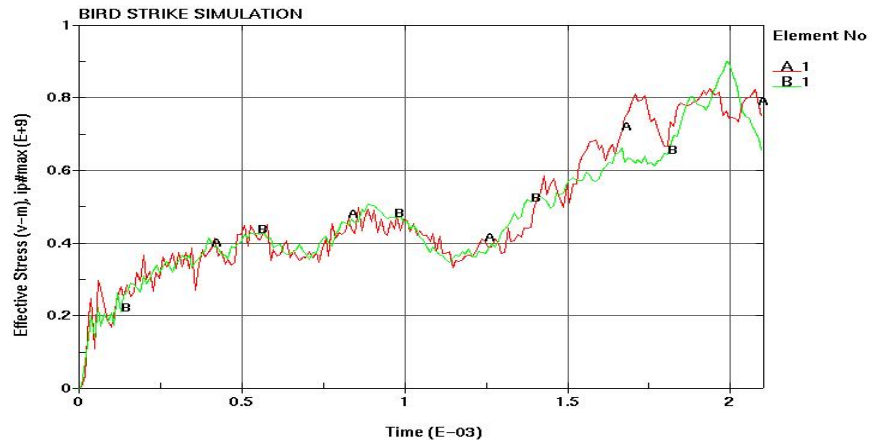


Figure G1: Effective Stress Plot (Lagrangian Model)  
(A for Coarser Mesh B for Denser Mesh)

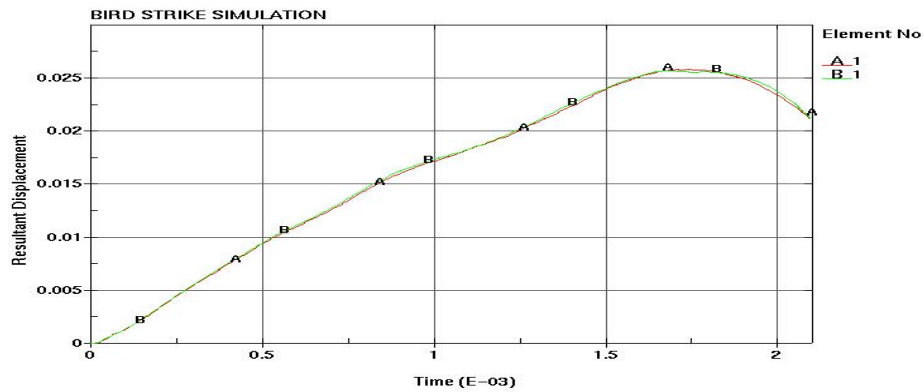


Figure G2: Resultant Displacement Plot (Lagrangian Model)  
(A for Coarser Mesh, B for Denser Mesh)

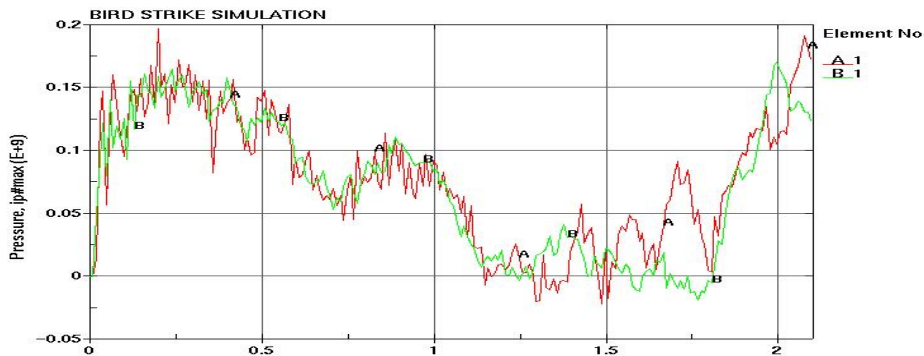


Figure G3: Pressure Plot (Lagrangian Model)  
(A for Coarser Mesh, B for Denser Mesh)

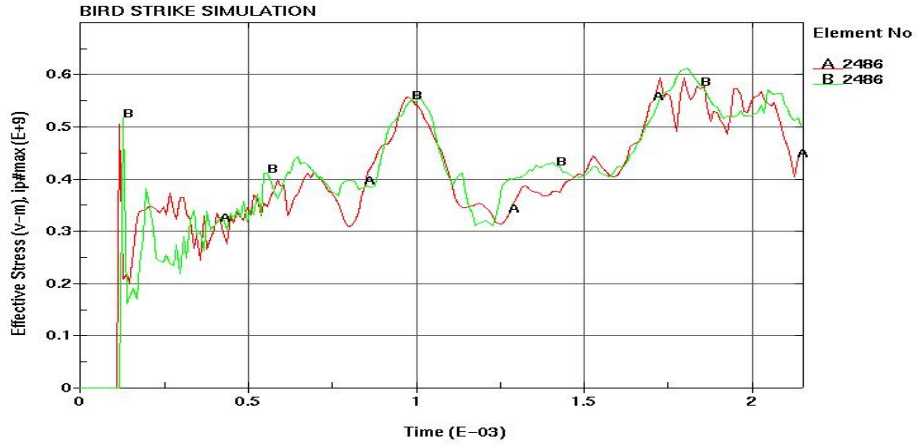


Figure G4: Effective Stress Plot (ALE Model)  
(A for Coarser Mesh B for Denser Mesh)

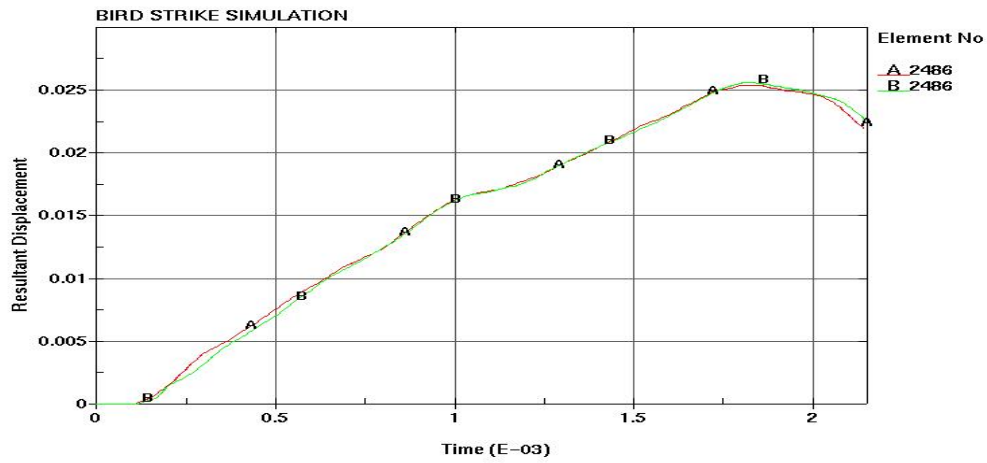


Figure G5: Resultant Displacement Plot (ALE Model)  
(A for Coarser Mesh, B for Denser Mesh)

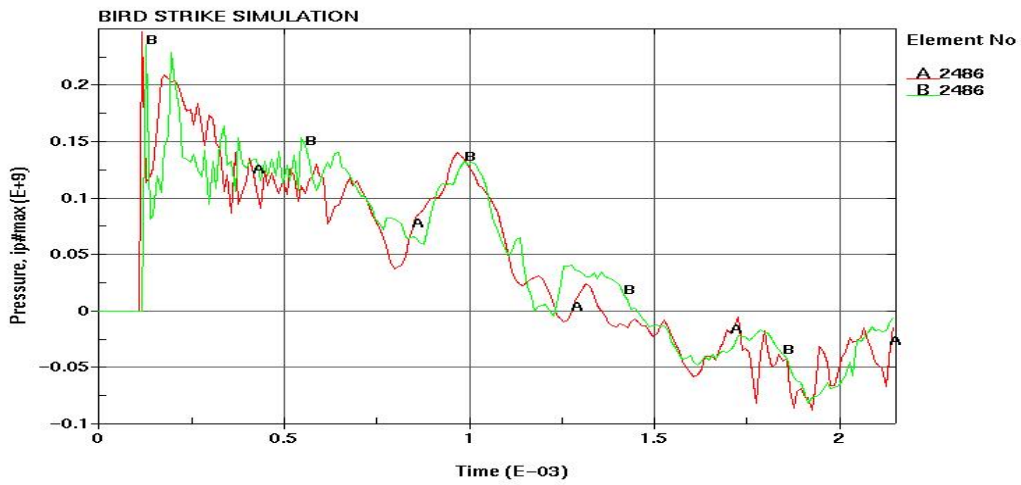


Figure G6: Pressure Plot (ALE Model)  
(A for Coarser Mesh, B for Denser Mesh)

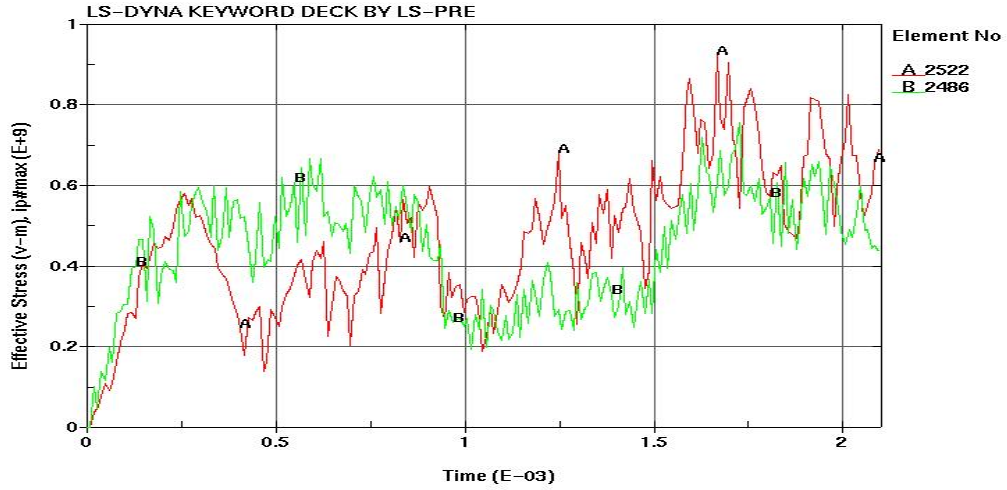


Figure G7: Effective Stress Plot (SPH Model)  
 (A for Lesser Particles B for More Particles)

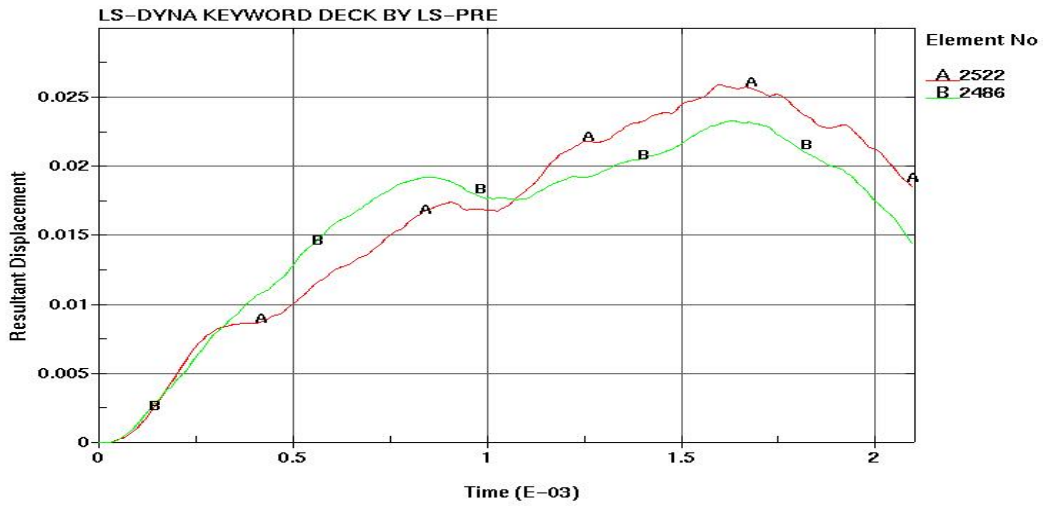


Figure G8: Resultant Displacement Plot (SPH Model)  
 (A for Lesser Particles, B for More Particles)

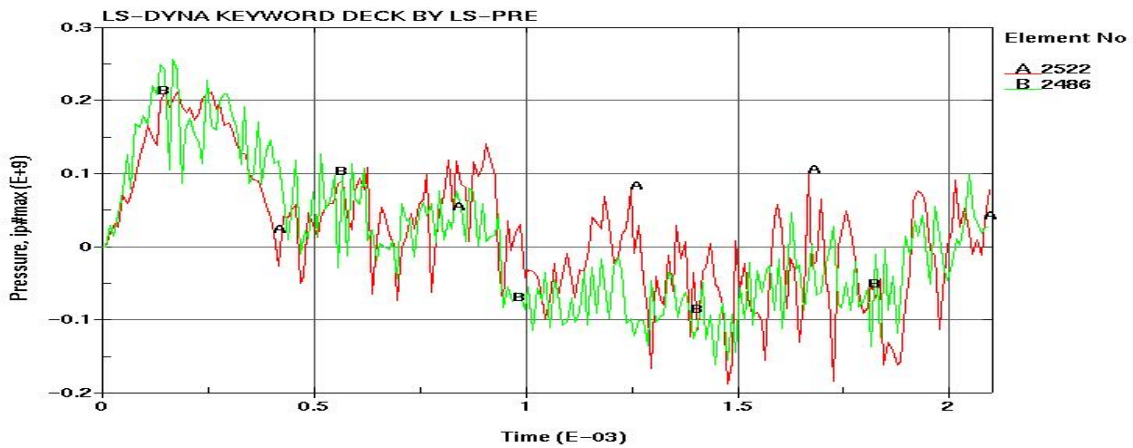


Figure G9: Pressure Plot (SPH Model)  
 (A for Lesser Particles, B for More Particles)

***APPENDIX H – EFFECTIVE STRESS OF  
TRANSPARENCIES WITH DIFFERENT  
CURVATURE***

Effective stress for transparencies of intermediate curvature between radius of curvature of 0.5m to infinity is plotted. The transparencies of the different curvature can be identified by the plate number as shown in table 3.7. Figure H1 to H3 shows the effective stress experienced by the outer, middle and inner layer of the transparencies with different curvature. Generally the gradual increase or decrease of the effective stress due to a change in the curvature can be observed.

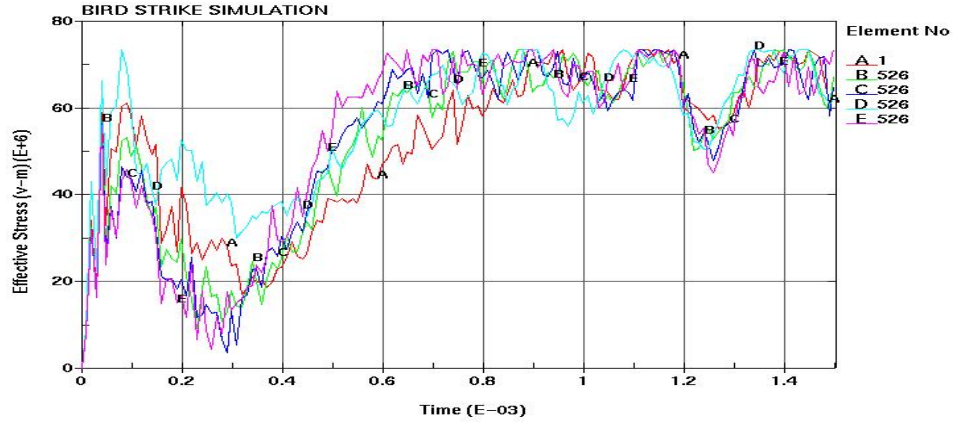


Figure H1: Effect of Curvature on Effective Stress (Outer Layer)  
 (A for plate2, B for plate3, C for Plate4, D for Plate 1, E for Plate 5)

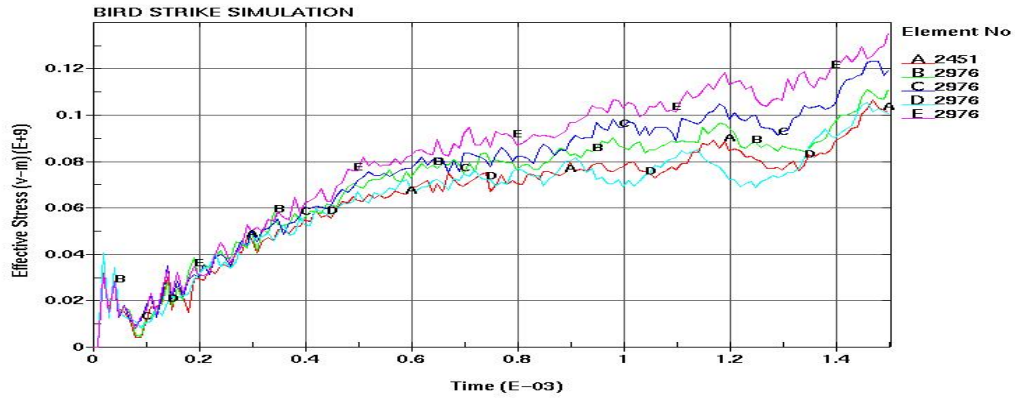


Figure H2: Effect of Curvature on Effective Stress (Middle Layer)  
 (A for plate2, B for plate3, C for Plate4, D for Plate 1, E for Plate 5)

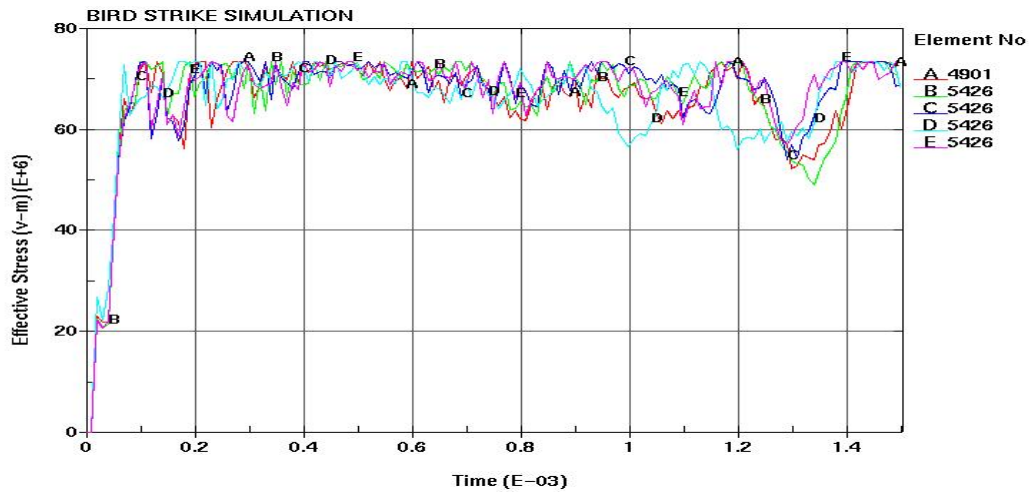


Figure H3: Effect of Curvature on Effective Stress (Inner Layer)  
 (A for plate2, B for plate3, C for Plate4, D for Plate 1, E for Plate 5)

***REFERENCES***

- 1) <http://www.birdstrike.org/commlink/birdrisk.htm>
- 2) Sharing the skies – An aviation industry guide to the management of wildlife hazards. Ottawa, Ontario: Transport Canada, Aviation Publishing Division, AARA, 2001.
- 3) <http://wildlife.pr.erau.edu/index.html>
- 4) Edward C. Cleary, Richard A. Dolbeer, Sandra E. Wright, Wildlife strike to civil aircraft in the united states 1990 – 2003; Federal Aviation Administration National Wildlife Strike Database Serial Report Number 10, June 2004
- 5) Wendy Servoss, Richard M Engeman, Steven Fairaizl, John L Cummings, N.Paige Groninger, Wildlife hazard assessment for phoenix sky harbor international airport, International Biodeterioration and Biodegradation 45 (2000) 111 - 127
- 6) <http://www.boeing.com/commercial/safety/whatmakes.html>
- 7) PAM-SHOCK<sup>TM</sup>/PAM-CRASH<sup>TM</sup> FE Code, Engineering Systems International, F-94578 Rungis Cedex, France.
- 8) LS-DYNA – Theoretical manual. : Livermore Software Technology Corporation, 1998
- 9) John P. Barber, et al, Characterization of bird impacts on a rigid plate (Part 1), Dayton University, National Technical Information Service U.S Department of Commerce, January 1975

- 
- 10) Alastair F. Johnson, Martin Holzapfel, Modeling soft body impact forces on composite structures, *Composite Structures* 61 (2003) 103 - 113
  - 11) A. Airolidi, B. Cacchione, Modeling of impact forces and pressures in Lagrangian bird analysis, *International Journal of Impact Engineering*, Vol. 32, Issue 10, 1651-1677, Oct 2006
  - 12) B Lagrand, A.s Bayard, Y Chauveau, E Deletombe, Assessment of multi-physics FE methods for bird strike modeling – Application to a metallic riveted airframe, *International Journal of Crashworthiness* 7(4), 2002, 415-428
  - 13) S. C. McCallum, C. Constantinou, Influence of bird-shape in bird strike analysis, 5<sup>th</sup> European LS-DYNA Users Conference
  - 14) M. A. McCarthy, J. R. Xiao, C. T. McCarthy, A. Kamoulakos, J. Ramos, J. P. Gallard, V. Melito, Modeling of bird strike on an aircraft wing leading edge made from fibre metal laminates – Part 2: Modeling of Impact with SPH bird model, *Applied Composite Materials* 11: 317 – 340, 2004
  - 15) A.F. Storace, R.P. Nimmer, R. Ravenhall, Analytical and Experimental investigation of bird impact on fan and compressor blading, *Journal of Aircraft*, Vol. 21: 520 – 527, 1998
  - 16) A.G. Hannsen, Y. Girard, L. Olovsson, T. Berstad, M. Langseth, A numerical model for bird strike of aluminum foam-based sandwich panels, *International Journal of Impact Engineering*, Vol. 32, Issue 7, 1127-1144, Jul 2006
  - 17) RADIOSS V4 USER MANUAL, Mecalog Holding, France
  - 18) L. Iannucci, Foreign object impact and energy absorbing structure, CHE Seminar Publication, 1998

- 19) G.R.Liu, S.S. Quek, The Finite element method, a practical course, 2003
- 20) Truegrid<sup>R</sup> Manual, Verson 2.0.0 Revision2, XYZ Scientific Applications, Inc,  
March 30, 2000
- 21) F. W. Flocker, L. R. Dharani, Stresses in laminated glass subject to low velocity  
impact, Engineering Structures, Vol19, No10, pp.851 – 856, 1997
- 22) Brent Wright, Benefit of acrylic and composite window for transport aircraft,  
Sierracin/Sylmar Corporation
- 23) <http://www.matweb.com/search/GetProperty.asp>